THE Journal OF THE AMERICAN LEATHER CHEMISTS ASSOCIATION

July 2023 Vol. CXVIII, No.7 *JALCA* 118(6), 269–312, 2023

Contents

Distributed by
University of CINCINNATI
LIBRARY PUBLISHING SERVICES

An imprint of the University of Cincinnati Press

ISSN: 0002-9726

Communications for Journal Publication

Manuscripts, Technical Notes and Trade News Releases should contact:
Mr. Steven D. Lange, Journal Editor, c/o University of Cincinnati, 5997 Center Hill Ave., Bldg. C, Cincinnati, OH 45224, USA
E-mail: jalcaeditor@gmail.com Mobile phone: (814) 414-5689

Contributors should consult the Journal Publication Policy at:
http://www.leatherchemists.org/journal_publication_policy.asp

Beamhouse efficiency takes perfect balance.

Making leather on time, on spec and within budget requires a careful balance of chemistry and process. Buckman enables tanneries to master that balance with our comprehensive Beamhouse & Tanyard Systems. They include advanced chemistries that not only protect the hide but also maximize the effectiveness of each process, level out the differences in raw materials and reduce variations in batch processing. The result is cleaner, flatter pelts. More uniform characteristics. And improved area yield.

In addition, we offer unsurpassed expertise and technical support to help solve processing problems and reduce environmental impact with chemistries that penetrate faster, save processing time, improve effluent and enhance safety.

With Buckman Beamhouse & Tanyard Systems, tanneries can get more consistent quality and more consistent savings. Maintain the perfect balance. Connect with a Buckman representative or visit us at **Buckman.com**.

1945 2020 Buckman75

JOURNAL OF THE
AMERICAN LEATHER CHEMISTS ASSOCIATION

Proceedings, Reports, Notices, and News
of the
AMERICAN LEATHER CHEMISTS ASSOCIATION

THE JOURNAL OF THE AMERICAN LEATHER CHEMISTS ASSOCIATION (USPS #019-334) is published monthly by The American Leather Chemists Association, c/o University of Cincinnati, 5997 Center Hill Ave., Bldg. C, Cincinnati, Ohio 45224. Telephone (513)290-2507. Single copy price: $10.00 members, $20.00 non-member plus shipping and handling. Subscriptions: $185 for hard copy plus postage and handling of $60 for domestic subscribers and $70 for foreign subscribers; $220 for ezine only; and $240 for hard copy and ezine plus postage and handling of $60 for domestic subscribers and $70 for foreign subscribers.

Periodical Postage paid at Cincinnati, Ohio and additional mailing offices. Postmaster send change of addresses to The American Leather Chemists Association, c/o University of Cincinnati, 5997 Center Hill Ave., Bldg. C, Cincinnati, Ohio 45224.

Website: www.leatherchemists.org E-mail: hallks@ucmail.uc.edu

COLD
Milling

Smooth Leather Milling

Erretre
Tannery Innovations

Erretre s.p.a. | Via Ferraretta,1 | Arzignano (VI) 36071 | tel. +39 0444 478312 | info@erretre.com

Study on Interaction Mechanism between Neutral Salts and Collagen by Combining Experiments with Molecular Dynamics Simulation

by
Min Gu,[1] Xiaoxia Zhang,[1] Yuanzhi Zhang,[1] Songcheng Xu[1] and Guoying Li[1,2*]
[1]*National Engineering Research Center of Clean Technology in Leather Industry, Sichuan University,* Chengdu 610065, China
[2]*Key Laboratory of Leather Chemistry and Engineering (Ministry of Education), Sichuan University,* Chengdu 610065, China

Abstract

The effect of salt on the collagen of hide/skin is of great significance in leather-making. However, the interaction between neutral salts and collagen has not been clear, since the microscopic interaction is hard to be observed directly from the macro level of hide/skin collagen. In this study, the collagen solutions in the typical neutral salts (NaCl, $CaCl_2$, and Na_2SO_4) systems were used to explore the interaction mechanism between neutral salts and collagen via combining experiments with molecular dynamics (MD) simulation. The results of fluorescence measurements of pyrene, dynamic light scattering, atomic force microscopy, and isoelectric point suggested that the variation of the interaction between different neutral salts and collagen was accompanied with the changes in physicochemical properties of collagen. MD simulation further revealed more detailed information on the interaction mechanism between neutral salts and collagen at the molecular level. The computational results of non-bond energy of the collagen-salt model boxes indicated that the electrostatic interactions of different salts with collagen molecules had the order of $CaCl_2$> Na_2SO_4> NaCl. The analyses of the visualized conformation and the radial distribution functions showed that $CaCl_2$ with Ca^{2+} as contributing ion tended to form intramolecular salt bridges with collagen, while Na_2SO_4 with SO_4^{2-} as contributing ion more likely formed salt bridges between collagen molecules in the shape of agglomerates. In contrast, NaCl with Cl^- as contributing ion was scattered around the collagen models, and its effect on collagen was much smaller. The study elaborated the interaction mechanism of typical neutral salts and collagen to be helpful for further understanding and improving the use of neutral salts in many steps involved in leather production.

Introduction

Neutral salts, as common chemicals used in leather production, play an important role in the production of leather with satisfactory mechanical, aesthetic and hygienic performance.[1] The effects of neutral salts on pelts in leather-making processes have been investigated, which were known as the salt effects such as avoiding undesirable swelling, dispersing fiber bundles, dehydrating, and reducing the thickness variance of pelts.[1-3] Although the effects of neutral salts in leather-making processes have been known, the underlying interaction mechanism between neutral salts and collagen in leather is not fully understood. Figuring out the interaction mechanism between neutral salts and collagen would be helpful to understand the roles of salts and provide guidance to make full use of salts in leather-making industry.

Collagen is the main structural component within leather and hide/skin in the form of high-level fiber bundles.[4-6] Since the microscopic interaction is hard to be directly observed from the macro level of hide/skin collagen fibers, collagen solution is a better option to explore the interaction mechanisms. The physicochemical properties of collagen, such as microstructure, thermal stability, isoelectric point, viscosity, fiber-forming properties, and so on, would be changed with the addition of neutral salts.[7-11] Wei et al. studied the microstructure of collagen molecules in NaCl solution to describe the role of NaCl in pickling and tanning processes.[12] The formation of an orderly and porous microstructure was observed via atomic force microscope (AFM) when NaCl was present in collagen solution, which was considered to help improve the penetration of tanning agents and the mechanical property of leathers.[12] Brown et al. investigated the effect of neutral salts on the hydrothermal stability of collagen, and the results suggested that the neutral salts appeared to bind to collagen via electrostatic interaction to decrease the hydrothermal stability of collagen.[13] Penkova et al. further detected the thermal stability of collagen varied with salt ion species as followed the order of $H_2PO_4^-$≥ SO_4^{2-}> Cl^-> SCN^-, indicating salts had different interactions with collagen.[14] Freudenberg et al. found that $CaCl_2$ shifted the isoelectric point of collagen to a higher pH, indicating calcium ions bound to the carboxyl groups of collagen molecules.[15] Duan et al. deduced that the decline of collagen viscosity at low concentrations of NaCl solutions was attributed to the change of interaction among collagen molecules due to the charge screening by chloride ions.[9] Li et al. proposed that the main interaction between multivalent ions and collagen was ion binding and the multivalent ions could change collagen surface charge after investigating the fiber-forming properties of collagen in various salts.[10] These studies have established an association between salts and the physicochemical

*Corresponding author email: liguoyings@163.com
Manuscript received December 13, 2022, accepted for publication February 27, 2023.

properties of collagen solutions, which suggested that neutral salts had electrostatic interactions with collagen molecules and the interactions between salts and collagen varied with salt species. However, the interaction mechanism between collagen and neutral salts is not completely clear, and there is little information about the interaction mechanism at molecular level.

Molecular dynamics (MD) simulation is an effective method to explore interaction mechanism of particles at molecular level.[16, 17] This technology can simulate various experimental conditions, such as changes in solvent, to understand the conformation changes and dynamic mechanisms of proteins.[18] At present, MD simulation has been increasingly applied in research on collagen to give insight into the microscopic interaction mechanisms of collagen under various conditions.[19, 20] Niu et al. explored the mechanism of collagen intrafibrillar mineralization via using MD simulation to analyze the movement data of water and ions in the collagen mineralization models in presence of polyelectrolyte ions.[20] Ding et al. performed MD simulation on a chrome tanning model containing collagen fibrils and polychromiums, and clearly described the cross-linking site, topology and capacity of the cross-linkage of polychromiums to peptide chains.[21] Bulo et al. built a collagen fibril model and simulated the pickling process to study the effects of neutral salts (NaCl, $CaCl_2$, and Na_2SO_4) on the swelling behavior of fibrils in pickling.[4] Through the RDF analysis, it confirmed that $CaCl_2$ and Na_2SO_4 had specific stabilizing effects on fibrils owing to the weak self-interaction of $CaCl_2$ and the strong interactions of SO_4^{2-} with the basic amino acid residues of fibrils, respectively.[4] These studies mainly used collagen fibril models for investigation, some detailed information at the molecular and atomic levels could not be obtained. And there are few studies using a collagen molecule model to investigate the interaction mechanism between salts and collagen. A MD simulation with a collagen molecule model would be helpful to explore the mechanism between neutral salts and collagen with a deep understanding.

In this study, the interaction mechanism between typical neutral salts (NaCl, $CaCl_2$, and Na_2SO_4) and collagen was investigated by combining experiments with MD simulation. Pyrene fluorescence spectra, dynamic light scattering (DLS) measurements, and AFM were applied to characterize the effect of the neutral salts on the intermolecular interactions between collagen molecules in different salt solutions based on the aggregation behaviors of collagen molecules. Zeta potential measurement was performed to detect the change of isoelectric point (pI). MD simulation with a collagen molecule model was performed to get some insight into the interaction mechanisms between neutral salts and collagen at molecular level, including energy calculation, conformation analysis and RDF calculation. The results were expected to further understand and improve the use of neutral salts in many steps involved in leather production.

Materials and Methods

Materials

Collagen was extracted from bovine hide following the method of Li et al. with a slight modification.[22] Briefly, after unhairing and defatting pretreatments, the dermis of bovine hide was cut into small pieces, and the pieces were dissolved in 0.5 mol/L acetic acid containing 3% pepsin (1:3000) at 4°C. Type I collagen was collected and purified from the supernatants by centrifuging, salting out, redissolving, dialyzing and lyophilizing. The collagen sponge was stored in a desiccator for use.

Pepsin and pyrene were purchased from Sigma Aldrich.

Preparation of Collagen Solutions with Salts

Lyophilized collagen was dissolved in 0.01 M acetic acid to obtain 1.0 mg/mL and 3.0 mg/mL collagen stock solutions. Then the 1.0 mg/mL collagen stock solutions were separately mixed with NaCl solutions at different concentrations at 4°C to finally obtain 0.5 mg/mL collagen sample solutions containing a series of NaCl concentrations (0, 40, 80, 120, 160, and 200 mM). The collagen sample solutions containing 0–200 mM $CaCl_2$ or Na_2SO_4 were similarly prepared by replacing NaCl with $CaCl_2$ or Na_2SO_4. The collagen sample solution containing 0 mM salt was used as the control, simply called pure Col, and the collagen sample solutions containing NaCl, $CaCl_2$ or Na_2SO_4 were called Col/NaCl, Col/$CaCl_2$, and Col/Na_2SO_4, respectively. These sample solutions were subjected for the subsequent measurements. And the 3.0 mg/mL collagen stock solutions were separately mixed with salt solutions to obtain 0.001–3.0 mg/mL collagen sample solutions containing 80 mM NaCl, $CaCl_2$, or Na_2SO_4, which were used for collagen critical aggregation concentration (CAC) measurements.

Measurements of Pyrene Fluorescence Spectra

Pyrene fluorescence spectra measurements were performed to characterize collagen aggregation state and determine the CAC of collagen. Fluorescence spectra measurements were performed according to the method of Yang et al with slight modifications.[23] Firstly, 50 μL 400 μM pyrene solution was introduced to a 25-mL brown glass volumetric flask and gently evaporated under a nitrogen gas stream. Then the collagen sample solutions (pure Col, Col/NaCl, Col/$CaCl_2$, and Col/Na_2SO_4) were separately added into the volumetric flasks and fully homogenized by an ultrasonic cleaner at 4°C. Before measurement, the solutions were kept in a dark place for 12 h at 4°C. Measurements were performed with a fluorescence spectrophotometer (F-7100, Cary Eclipse, Agilent, Santa Clara, California) at 25°C. All samples were excited at 343 nm, and the emission spectra were collected from 360 to 460 nm with a scanning rate of 240 nm/min. In the measurements, the slits opening of excitation and emission were fixed at 5 nm and 2.5 nm, respectively. All fluorescence measurements were performed in triplicate.

Measurements of Dynamic Light Scattering

Dynamic light scattering (DLS) measurements were carried out for the size distribution of the collagen solutions. After being transferred to polystyrene cuvettes, the 0.5 mg/mL collagen solutions containing 0–200 mM salts were immediately determined by a Zetasizer instrument (Nano-ZS, Malvern, UK) with an angle detection of 90° at 25°C. All DLS measurements were carried out in triplicate.

Atomic Force Microscope Measurements

The 0.5 mg/mL collagen solutions containing 0–200 mM salts were diluted to 25 μg/mL for AFM measurements. Droplets of the diluted solutions were immediately dropped on freshly cleaved mica sheets and then dried at room temperature for 48 h in air. The microstructure of the dried samples was observed by AFM (Shimadzu SPM 9600, Kyoto, Japan) in the soft tapping mode with a scanning rate of 1HZ.

Measurements of Zeta Potential

The 0.5 mg/mL collagen solutions containing 0 mM and 80 mM salts were determined for zeta potential. Firstly, the pH of these solutions was adjusted to 4~11 with 0.2 M NaOH under ice-bath conditions. Then, these solutions were immediately measured for the zeta potential by a Zetasizer instrument (Nano-ZS, Malvern, UK) at 25°C. The Smoluchowski model was chosen to calculate the zeta potential. Each sample was determined in triplicate.

Constructions of Collagen Model and Simulation Boxes

Collagen molecule model and simulation box constructions, and molecular dynamics (MD) simulation were performed by the Materials Studio, version 6.0 software package (Key Laboratory of the Ministry of Education for Advanced Catalysis Materials, Institute of Physical Chemistry, Zhejiang Normal University, Zhejiang, China).

The amino acid sequence of bovine hide type I collagen was retrieved from the UniProtKB database (entry: P02453(α1), P02465(α2)). Due to the big length of the collagen chains, we selected a fragment of the collagen chains as natural collagen molecule model based on the content of ionizable amino acids, and its amino acid sequence was listed:

α_1→GEQGVPGDLGAPGPSGARGERGFPGERGVQ

α_2→GERGIPGEFGLPGPAGARGERGPPGESGAA

α_1→GEQGVPGDLGAPGPSGARGERGFPGERGVQ

The collagen molecule model was constructed according to the method of the previous work in our lab with a slight modification.[24] The basic amino acid residues of the model were protonated and the acidic amino acid residues were dissociated accompanied with 12 free H^+ in order to accelerate the interactions between salts and the collagen model. The model was further refined by geometry optimization with a smart algorithm in Forcite module. H_2O, CH_3COO^-, H^+ and salt ions (Na^+, Cl^-, Ca^{2+}, and SO_4^{2-}) were also built and geometry optimized.

The final simulation system for the control group (simply called [pure Col] system) consisted of a collagen model, 3 CH_3COO^-, 15 H^+, and 500 H_2O, and they were randomly placed in a cubic box with a density of 1 g/cm^3 by Amorphous cell module. NaCl, $CaCl_2$, and Na_2SO_4 were added and randomly dispersed into the [pure Col] system to constitute the corresponding systems, simply called [Col/NaCl], [Col/Na_2SO_4] and [Col/$CaCl_2$] systems, respectively, and the number of salts added to each system was 20. The simulation boxes were geometry optimized by Forcite module.

Molecular Dynamics Simulation

To investigate the interaction mechanism between the salts and collagen, the MD simulations with an NPT ensemble (298.15 K and 1 atm) were carried out by Forcite module. The Dreiding force field was applied in the simulation, and the Berendsen barostat and the Nose-Hoover thermostat were used to keep the pressure and temperature constant, respectively. The MD simulations consisted of two simulations, the first one for an equilibration run and the latter one with 50 000 steps for a production run. All analyses were calculated based on the production run. The non-bond energy of collagen models in different salt systems was calculated and the conformations of collagen models in each system were used to analyze the interactions between collagen models and salt ions. The final 500 ps trajectories of the production run were for radial distribution function (RDF) analysis which could describe the distribution of the salt ions and water molecules around the collagen model. The RDFs of the collagen model with salt ions and water were obtained by choosing corresponding particles as the sets to calculate, and the cutoff distance between the sets for RDFs was 30 Å.

Results and Discussion

Pyrene Fluorescence Spectra Analysis

As a sensitive hydrophobic fluorescent probe, pyrene can be used to measure the polarity of the microenvironment of solutions.[25] Since collagen aggregation was accompanied by the formation of hydrophobic microdomains where pyrene was located, pyrene fluorescence spectra can be employed to characterize collagen aggregation behaviors and intermolecular interactions in solutions.[23]

Figure 1A1–A3 shows the pyrene fluorescence emission spectra of 0.5 mg/mL collagen solutions containing 0–200 mM salts (NaCl, $CaCl_2$, and Na_2SO_4). The spectra display the four characteristic peaks at 374,

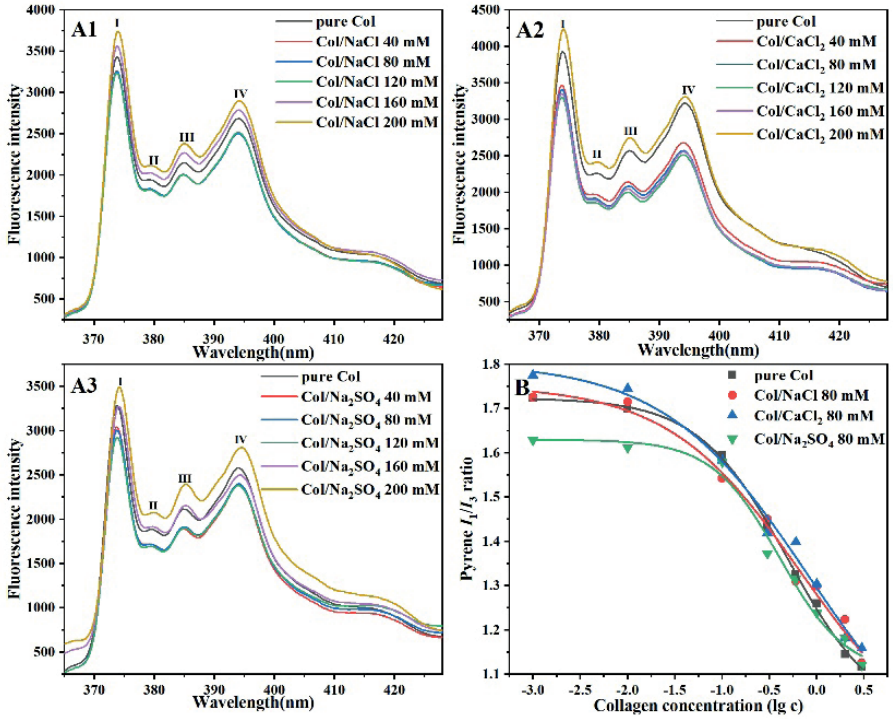

Figure 1. Pyrene fluorescence emission spectra in 0.5 mg/mL collagen solutions containing 0–200 mM salts (**A1**–**A3**). **A1**, Col/NaCl; **A2**, Col/$CaCl_2$; **A3**, Col/Na_2SO_4. Plots of the pyrene I_1/I_3 ratio versus the logarithm of the collagen concentration in 0 mM and 80 mM salts (NaCl, $CaCl_2$, and Na_2SO_4) solutions at 25°C (**B**).

380, 385 and 394 nm, indicating pyrene was stable in solutions.[25] The intensity ratio of the first to the third vibronic peaks (I_1/I_3) could be regarded as a polarity index.[25] The I_1/I_3 values of the collagen solutions containing 0–200 mM salts are listed in Table I. From Table I, we found that in all studied salt solutions, with increasing salt concentration, the I_1/I_3 values first increased, suggesting the decrease of the hydrophobic microdomains, which was correlated with the disaggregation of collagen molecules and the weak intermolecular interactions. However, with further increasing salt concentration, the I_1/I_3 values turned to decrease, indicating the enhancement of collagen aggregation and intermolecular interactions. Besides salt concentration, the I_1/I_3 values and aggregation behaviors were also affected by salt species. It was noted that the fewest hydrophobic microdomains and weakest aggregation behavior of collagen molecules were at the salt concentrations of 40 mM for Na_2SO_4, 120 mM for NaCl and 160 mM for $CaCl_2$, respectively. Compared with the I_1/I_3 values in Col/NaCl, Col/$CaCl_2$, and Col/Na_2SO_4 at the same salt concentration, it was speculated that the collagen aggregation degree and interactions with salts in salt solutions had the order of Na_2SO_4> NaCl> $CaCl_2$. Furthermore, the order was consistent with the ability of these salts to suppress acid swelling in leather-making, which may be explained by that the salts at high concentrations enhanced collagen intermolecular interactions, promoted collagen aggregation, made water between collagen molecules out and then led to suppress pelts swelling. NaCl had a relative moderate ability to promote aggregation, so it was often used to suppress swelling, while Na_2SO_4 was used to dehydrate pelts and $CaCl_2$ was mainly used to disperse fibers of leather.[1] From the results, it was concluded that collagen aggregation behavior was affected by the concentration and species of salts and the salts affected the electrostatic and hydrophobic interactions of collagen molecules since aggregation was the result of these interactions.

Table I

The I_1/I_3 Ratio Values of Pyrene in 0.5 mg/mL Collagen Solutions Containing 0–200 mM Salts (NaCl, $CaCl_2$ and Na_2SO_4) and the CAC Values of Collagen in 0 mM and 80 mM Salts

Salt concentration (mM)	pure Col	Col/NaCl	Col/$CaCl_2$	Col/Na_2SO_4
0	1.599±0.005	1.599±0.005	1.599±0.005	1.599±0.005
40	/	1.613±0.001	1.621±0.004	1.605±0.003
80	/	1.617±0.002	1.632±0.004	1.569±0.004
120	/	1.621±0.001	1.644±0.001	1.538±0.004
160	/	1.571±0.004	1.648±0.005	1.525±0.003
200	/	1.497±0.007	1.542±0.005	1.456±0.004
CAC (mg/mL)	0.502	0.667	0.816	0.402

In order to further characterize the different effects caused by salt species, the CAC values of collagen in 0 mM and 80 mM salts were determined by pyrene fluorescence spectra method. The fluorescence spectra of 0.001–3.0 mg/mL collagen solutions with 80 mM salts also showed the characteristic peaks of pyrene (data not shown). The plots of the I_1/I_3 values versus the logarithm of the collagen concentration in different salts are presented in Figure 1B. By curve fitting the plots with a Boltzmann function, the concentration where the I_1/I_3 value was 50% of the initial I_1/I_3 value could be regarded as the CAC of collagen.[23] The CAC values of collagen in 0 mM and 80 mM salts are summarized in Table I. The CAC of pure Col was 0.502 mg/mL, consistent with the result of Yan et al.[25] The CAC values of collagen with 80 mM NaCl, $CaCl_2$, and Na_2SO_4 were 0.667, 0.816, and 0.402 mg/mL, respectively, indicating at 80 mM salt concentration, collagen molecules were induced to aggregate by Na_2SO_4, disperse slightly by NaCl and strongly disperse by $CaCl_2$. And it further indicated that at 80 mM, collagen intermolecular interactions were enhanced by Na_2SO_4, weakened slightly by NaCl and strongly weakened by $CaCl_2$, which implied collagen molecules had different interaction mechanisms with different salts.

Dynamic Light Scattering (DLS) Analysis

DLS can characterize the size distribution of collagen molecules and aggregates in salt solutions (NaCl, $CaCl_2$, and Na_2SO_4). Figure 2 displays the size distribution of 0.5 mg/mL collagen solutions containing 0–200 mM salts. All collagen solutions show two distribution ranges with values of 10–150 nm (called region A) and 460–2670 nm (called region B), which might be ascribed to the collagen aggregates with various sizes and the rod-like shape of collagen molecule.[26] Changes in the range and intensity of the two regions were observed in these sample solutions. For Col/NaCl (Figure 2B1–B5), the intensity of region B decreased and region B shifted to a smaller size region when NaCl concentration increased from 0 mM to 120 mM. Whereas, when NaCl further increased to 200 mM, the changes in size distribution were opposite to the above changes. It indicated that NaCl induced the disaggregation of collagen aggregates at 40–120 mM, but at higher concentrations (160–200 mM) NaCl promoted aggregation due to the enhanced collagen interactions. In Figure 2C1–C4 (Col/$CaCl_2$), region B obviously shifted to a smaller size region with increasing $CaCl_2$ concentration, indicating collagen was dispersed by 40–160 mM $CaCl_2$, which was ascribed to the increase of electrostatic repulsions between collagen molecules. Figure 2D2–D5 (Col/Na_2SO_4) shows the regions A and B both shifted to regions with larger particle sizes as Na_2SO_4 concentration increased, suggesting that Na_2SO_4 enhanced collagen interactions and promoted aggregation. The intensity of region B slightly reduced, which might be deduced that the formation of larger aggregates was accompanied with the disaggregation of some aggregates. The DLS results agreed with the results of pyrene fluorescence spectra. From the aspect of the aggregates size distribution, DLS results directly confirmed that collagen aggregation behavior and interactions could be modulated by these salts.

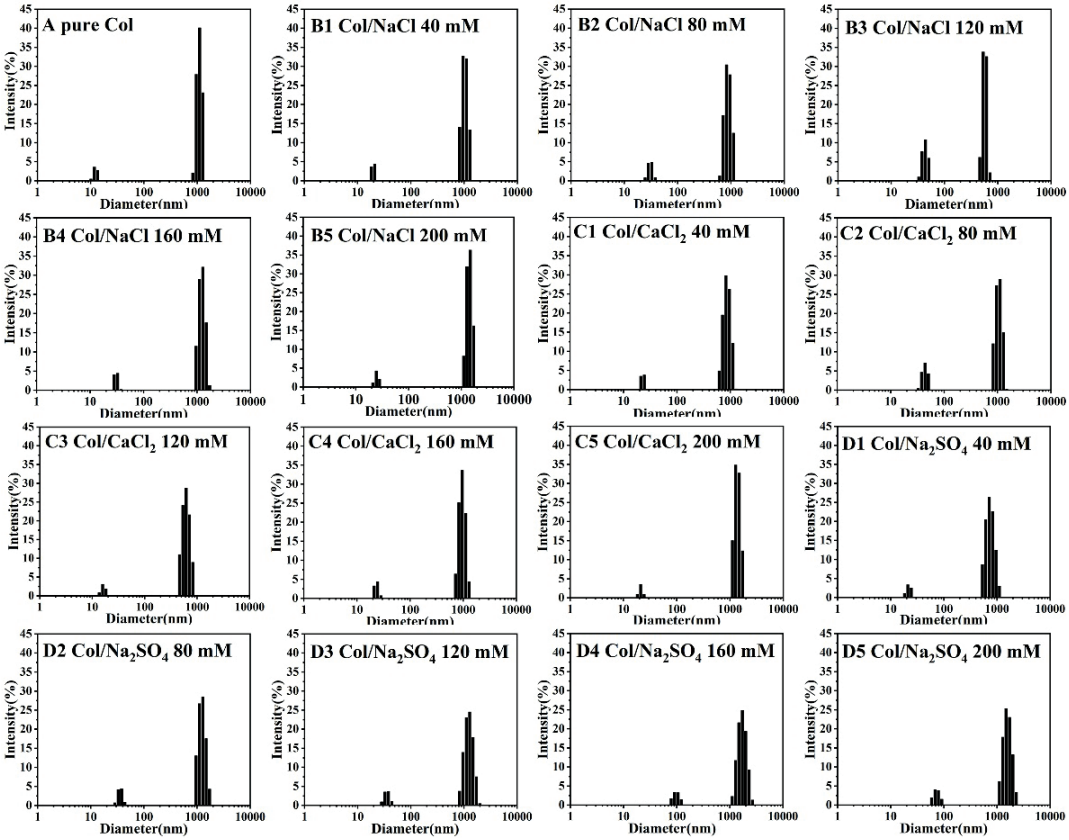

Figure 2. The size distribution of 0.5 mg/mL collagen solutions containing 0–200 mM salts by DLS at 25. **A**, pure Col; **B1–B5**, Col/NaCl; **C1–C5**, Col/$CaCl_2$; **D1–D5**, Col/Na_2SO_4.

Atomic Force Microscope (AFM) Images

Figure 3 displays the AFM images and morphological changes of collagen in 0–200 mM salt solutions. The collagen concentration (0.5 mg/mL) was close to collagen CAC (0.502 mg/mL), so it could be observed that some collagen molecules entangled with each other and aggregated in Figure 3A. Figure 3B1–B3 shows a disordered and loose morphology of collagen at 40–120 mM NaCl, while with more NaCl, collagen molecules were induced to entangle tightly and form orderly aggregates with spaces in Figure 3B4–B5. Wei et al. reported a similar phenomenon and ascribed it to the dehydration effect of NaCl.[12] Compared with NaCl, $CaCl_2$ induced collagen molecules to form dispersed loose porous networks in Figure 3C1–C4, and the porous structure was obvious in Figure 3C5, suggesting $CaCl_2$ had a dispersing effect on collagen. While Col/Na_2SO_4 presented tight entanglements with larger diameter of aggregates as presented in Figure 3D2–D5, especially obvious in Figure 3D5, indicating collagen interactions and aggregation were enhanced by Na_2SO_4. It was interesting to find that the morphology of collagen in different salts observed by AFM corresponded to the different effects of salts in leather-making. The AFM results were kept in line with the results of the fluorescence and DLS, and it suggested that NaCl, $CaCl_2$ and Na_2SO_4 had different effects on the micromorphology of collagen aggregates and interactions.

Zeta Potential Analysis

Zeta potential measurements were conducted to determine isoelectric point (pI) of collagen and further study the electrostatic interactions of collagen molecules in presence of salts. Figure 4 presents the zeta potential and pI of collagen in 0 mM and 80 mM salt solutions. The pI of pure Col was 7.5, similar to the result of Freudenberg et al.,[15] and the pI values of Col/NaCl, Col/$CaCl_2$, and Col/Na_2SO_4 at 80 mM salt concentration were 6.4, 10.8 and 5.5, respectively. The pI and surface charge of collagen were greatly affected by salt species, and the effect of $CaCl_2$ and Na_2SO_4 on pI was similar to the result of Li.[10] The change of pI was correlated with the preferential adsorption and binding of salt ions on collagen molecules.[10, 15, 27] The decreases of pI by NaCl and Na_2SO_4 implied that collagen mainly interacted with Cl^- of NaCl and SO_4^{2-} of Na_2SO_4. The preferential adsorption and binding of Cl^- and SO_4^{2-} on the positively charged residues of collagen, such as amino groups, reduced the positive charge of collagen, which led to the decrease of pI. At the same time the binding of the negative salt ions (Cl^- and SO_4^{2-}) to collagen could weaken the electrostatic repulsion between collagen molecules and promote collagen aggregation. On the contrary, the increase of pI by $CaCl_2$ implied that collagen had a preferential binding with positive Ca^{2+} of $CaCl_2$. The preferential binding of Ca^{2+} on the negatively charged residues of collagen, such as carboxyl groups, reduced the

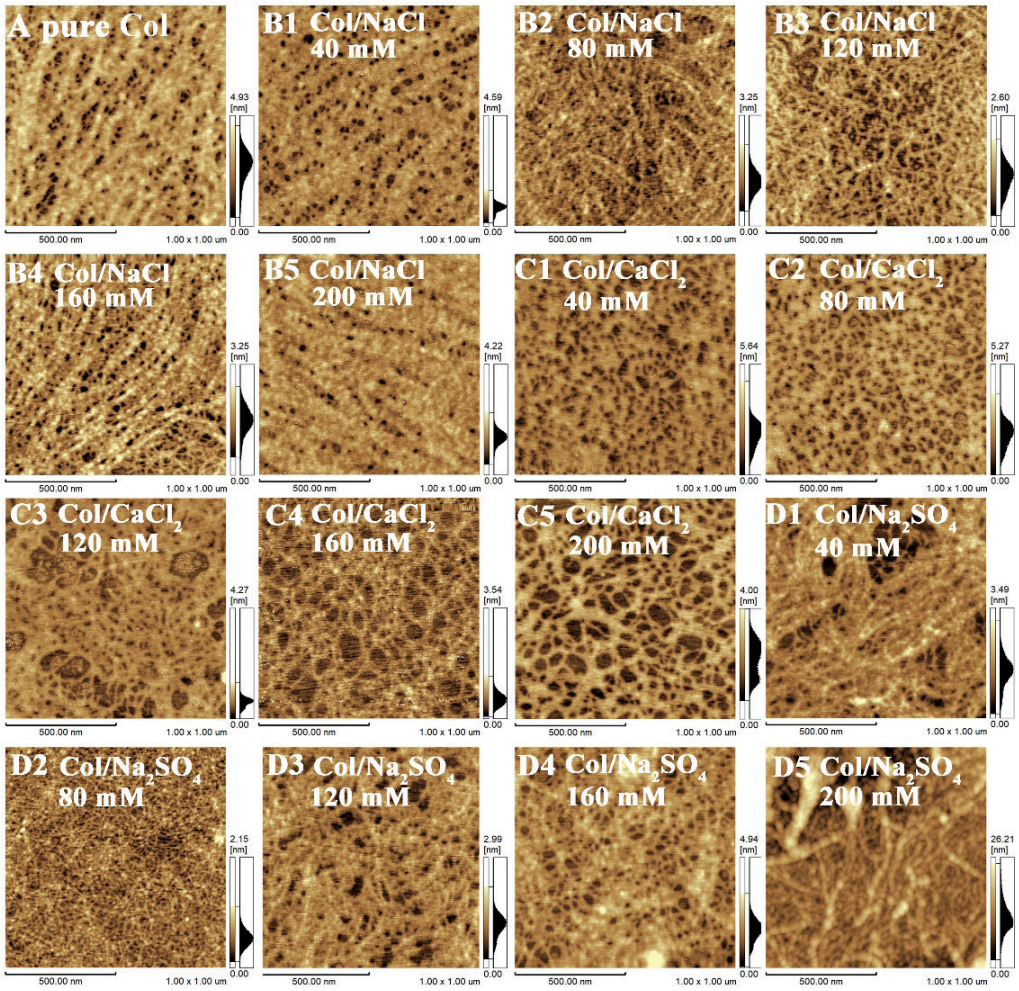

Figure 3. AFM height images of 0.5 mg/mL collagen solutions with 0–200 mM salts. **A**, pure Col; **B1–B5**, Col/NaCl; **C1–C5**, Col/$CaCl_2$; **D1–D5**, Col/Na_2SO_4.

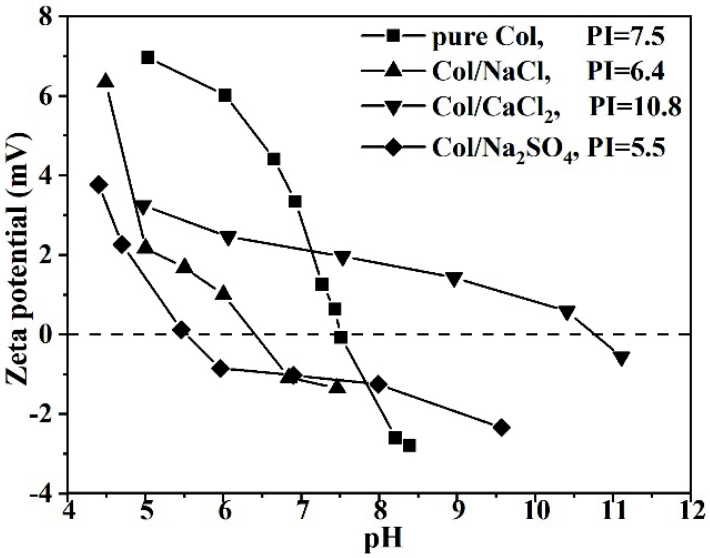

Figure 4. Zeta potential measurement of collagen in 0 mM and 80 mM salt solutions at 25°C.

negative charge of collagen, which led to the increase of pI. The binding of Ca^{2+} could enhance the electrostatic repulsion and inhibit aggregation. Compared with the monovalent salt ions (Na^+ and Cl^-), the divalent salt ions (Ca^{2+} and SO_4^{2-}) had stronger interactions with collagen because the change of pI in Col/$CaCl_2$ and Col/Na_2SO_4 was bigger than that in Col/NaCl.

Non-bond Energy Analysis in Different Salt Systems

The interactions between salts and collagen are non-bond interactions which include hydrogen bond, van der Waals and electrostatic interaction, so we calculated non-bond energies of collagen models in different salt systems to study the interactions between salts and collagen. The non-bond energies of collagen models in different salt systems are listed in Table II. As shown in Table II, the total non-bond energy of collagen models in salt systems was lower than that in [pure Col] system, and the non-bond energies including hydrogen bond, van der Waals and electrostatic energies of collagen models were affected by the salts. Also, it was observed that the change in electrostatic energy was bigger than the change in other non-bond energies, indicating the salts interacted with collagen mainly via electrostatic interactions. The magnitude of the effects of salts on electrostatic energy was ranked as NaCl< Na_2SO_4< $CaCl_2$, which was consistent with the magnitude of changes in the pI result.

Interactions between Collagen and Salts by Conformation Analysis

Molecular dynamics (MD) simulation is an effective tool to explore the interactions of collagen molecules with salt ions at molecular level and the conformation analysis from MD simulation can make the interactions visualized.[16, 17] The conformations of the different salt systems at the end of the simulation run are shown in Figure 5. The water molecules are not shown for a better visual effect, and there are two collagen models in each conformation because two boxes are displayed.

Figure 5 shows that in all salt systems, salt ions were around collagen models and had electrostatic interactions with collagen model. It was found that the salt ions bridged the acidic amino acid residues and basic amino acid residues of collagen molecules by intramolecular and intermolecular salt bridges, labeled in purple and red circles, respectively. In [Col/NaCl] system (Figure 5A), salt ions were scattered around collagen model, and there was an intermolecular salt bridge formed between the collagen models. By magnifying the intermolecular salt bridge in the red rectangle, we observed that Cl^- mainly interacted with the amino groups of collagen models to form salt bridges. The binding of Cl^- to collagen and the salt bridges could promote collagen interactions and aggregation. Figure 5B shows that in [Col/$CaCl_2$] system, Ca^{2+} and Cl^- wrapped around the collagen models with a line shape, and salt ions tended to form intramolecular salt bridges which was not beneficial for the interactions between collagen models. An intermolecular salt bridge was formed by $CaCl_2$ and Ca^{2+} mainly interacted with the carboxy groups of collagen models. The binding of positive Ca^{2+} to collagen enhanced the electrostatic repulsions between collagen models and then promoted collagen dispersion. In [Col/Na_2SO_4] system (Figure 5C), the salt ions formed clusters between the collagen models, and SO_4^{2-} mainly interacted with collagen models. Compared with NaCl and $CaCl_2$, Na_2SO_4 tended to form more intermolecular salt bridges between collagen molecules in the shape of agglomerates, indicating that Na_2SO_4 had a stronger ability to form intermolecular salt bridges and promote collagen aggregation. And the negative SO_4^{2-} directly interacted with the amino groups of collagen models, which could screen the positive charge of collagen and reduce electrostatic repulsion, as same as the results reported by Mertz et al.[28] Therefore, Na_2SO_4 could enhance collagen interactions and

Table II

Non-bond Energies (kcal/mol) of Collagen Model in [pure col] System and Different Salt Systems

System	Total non-bond energy	Hydrogen bond	van der Waals	Electrostatic energy
[pure Col]	-5657.619	-1591.960	789.922	-4855.581
[Col/NaCl]	-9439.522	-1553.262	917.032	-8803.292
[Col/$CaCl_2$]	-16944.006	-1622.528	1507.496	-16828.974
[Col/Na_2SO_4]	-15750.372	-1691.213	1035.209	-15094.369

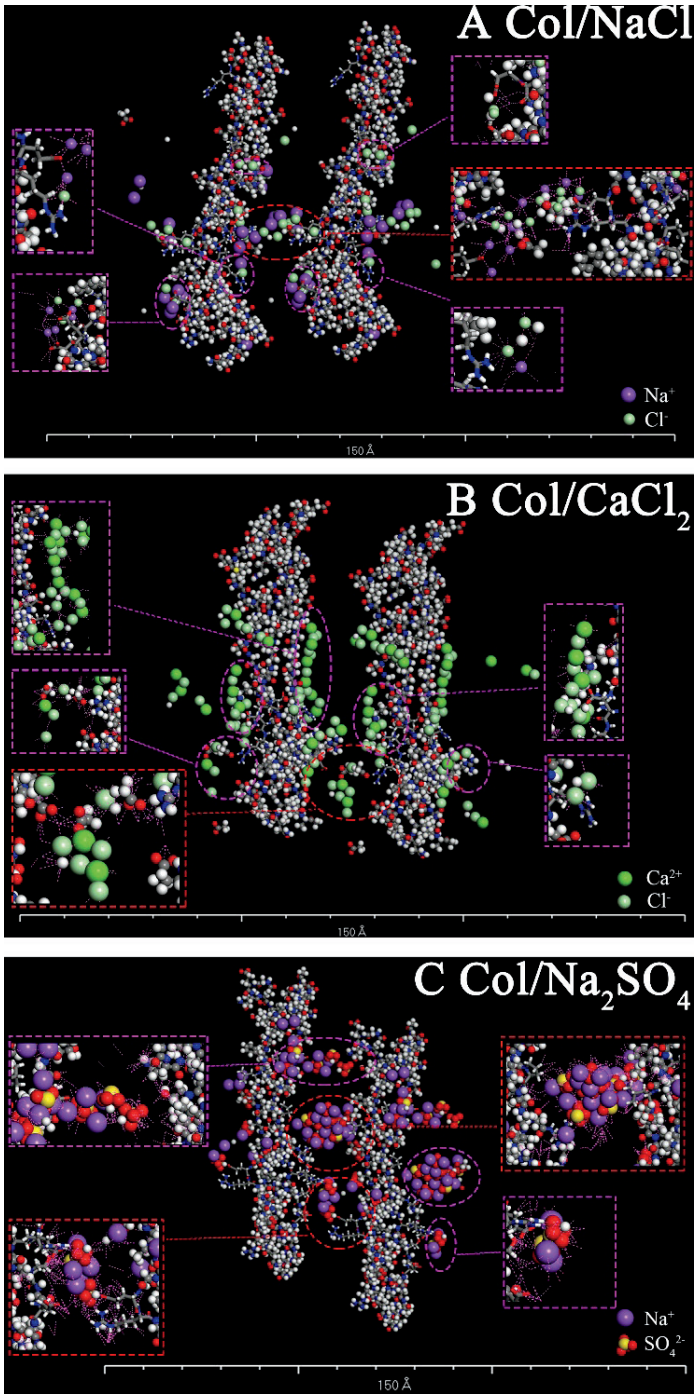

Figure 5. Conformations of collagen model in various salt systems. **A**, [Col/NaCl] system; **B**, [Col/$CaCl_2$] system and **C**, [Col/Na_2SO_4] system. Red and purple circles represented intermolecular and intramolecular salt bridges, respectively. Pink dashed lines represented electrostatic interactions.

promote aggregation due to enough intermolecular salt bridges formed in the shape of agglomerates and the screening charge effect of SO_4^{2-}.

Radial Distribution Function Analysis

Radial distribution function (RDF) is often used to analyze interactions of particles in simulation because it can describe the distribution and densities of the selected particles appearing around the collagen model.[29] The RDF values are positively correlated with the densities of the particles and they are normalized by the average densities.[4] We calculated RDFs to study the interactions between salts and collagen and the effect of salts on the hydration shell of collagen molecules.

The RDFs of Collagen–salt ions describe the distributions of salt ions around the charged amino acid residues (Glu, Asp and Arg) of the collagen model and they are shown in Figure 6A1–C2. All of the Collagen–salt ions RDFs had a peak within a distance of 5 Å and the peak values were much larger than 1, suggesting these salt ions were around the ionizable amino acid residues of collagen and had strong electrostatic interactions with the amino acid residues. In [Col/NaCl] system, the density of Cl^- around collagen was higher than that of Na^+ around collagen by comparing the peak values in Figure 6A1 and A2, indicating Cl^- of NaCl was the contributing ion for the interaction with collagen. The interaction of Cl^- with collagen was also reported by Bersusan et al.[30] Similarly, it could be inferred from Figure 6B1–C2 that Ca^{2+} of $CaCl_2$ and SO_4^{2-} of Na_2SO_4 were the contributing ions, and there were some studies reported the strong interaction of SO_4^{2-} with the charged moieties of amino acids.[28, 31] The density of Na^+ around collagen in [Col/NaCl] system (Figure 6A1) was higher than that in [Col/Na_2SO_4] system (Figure 6C1), which could be deduced that SO_4^{2-} had stronger interactions with collagen than Cl^-. Similarly, the noticeable decreased density of Cl^- in the [Col/$CaCl_2$] system (Figure 6B2) suggested Ca^{2+} had stronger interactions with collagen than Na^+. It seemed that divalent salt ions had greater effects on collagen than monovalent salt ions, which was supported by the electrostatic energy result. The results of contributing ions based on RDFs were consistent with the pI results. Since the contributing ions of NaCl and Na_2SO_4 were anions, the electrostatic repulsions between collagen molecules could be weakened by the screening charge effect of salt anions, and Na_2SO_4 had a stronger ability to promote collagen interactions than NaCl. $CaCl_2$ could enhance collagen electrostatic repulsions by the binding of positive Ca^{2+} to collagen and then disperse collagen.

The RDFs of Collagen–H_2O describe the distribution of water molecules around the collagen model in different systems and they are shown in Figure 6D–G. In [pure Col] system (Figure 6D), the first peak with a value bigger than 1 was at 3.19 Å, indicating water molecules were likely to appear around collagen molecules at this distance and it corresponded to the position of the first hydration

shell of collagen molecules. In [Col/NaCl] system (Figure 6E), the first hydration shell of collagen molecules shifted to a closer distance from collagen, at 2.93 Å, and the first peak value was larger than that in the [pure Col] system. It suggested that NaCl increased the density of water in the first hydration shell of collagen, which was the result of the weakened interactions between collagen models by NaCl. A similar change of the first peak was found in Figure 6F, and the change was more noticeable. Figure 6F suggested that $CaCl_2$ made the first hydration shell of collagen shift to 2.03 Å and observably enhanced the density of water around collagen. $CaCl_2$ had a bigger effect on the enhancement of the hydration shell of collagen than NaCl, indicating collagen molecules were more dispersed in $CaCl_2$ solution than in NaCl solution. The strong solvation effect of Ca^{2+} was also reported by Bulo et al.[4] Contrary to NaCl and $CaCl_2$, as depicted in Figure 6.G, Na_2SO_4 reduced the density of water in the first hydration shell of collagen and then excluded the water to a farther distance from collagen, at 11.79 Å, which corresponded to the position of the second hydration shell. It may be attributed to that Na_2SO_4 enhanced collagen intermolecular interactions, which made water move outward. The results of Collagen–H_2O RDF suggested that the density of water in the first hydration shell of collagen was increased a little by NaCl and clearly increased by $CaCl_2$, while clearly decreased by Na_2SO_4, which was correlated with different interactions of the salts with collagen.

The interaction mechanism between typical neutral salts (NaCl, $CaCl_2$, and Na_2SO_4) and collagen was investigated, which was helpful for understanding the different roles of the salts in leather-making. The results revealed that Ca^{2+} of $CaCl_2$, SO_4^{2-} of Na_2SO_4, and Cl^- of NaCl were the contributing ions for the interactions of the salts with collagen. $CaCl_2$ tended to form intramolecular salt bridges with collagen and the binding of Ca^{2+} enhanced the electrostatic repulsions among collagen molecules, which could widen the distance between collagen molecules and induce collagen to form loose porous networks. At the same time, more water was attracted to appear around collagen in the presence of $CaCl_2$. Then, as a result, collagen fibers and fiber bundles could be dispersed and opened up by $CaCl_2$. Gao et al. also reported that Ca^{2+} could widen the distance between fibers and disperse fibers, but Ca^{2+} also could make fibers swell and expand.[32] Na_2SO_4 obviously promoted collagen aggregation owing to clustered intermolecular salt bridges formed between collagen molecules and the weakened electrostatic repulsions by binding of SO_4^{2-}. Na_2SO_4 induced collagen to aggregate tightly, which could make water between collagen move outward, so Na_2SO_4 could dehydrate collagen fibers and fiber bundles. Owing to the strong ability of Na_2SO_4 to dehydrate and promote aggregation, fibers and fiber bundles might be not fully dispersed. Zhang et al. found that the opening effect of SO_4^{2-} on fiber bundles was not satisfying.[33] Compared with $CaCl_2$ and Na_2SO_4, NaCl had a moderate ability

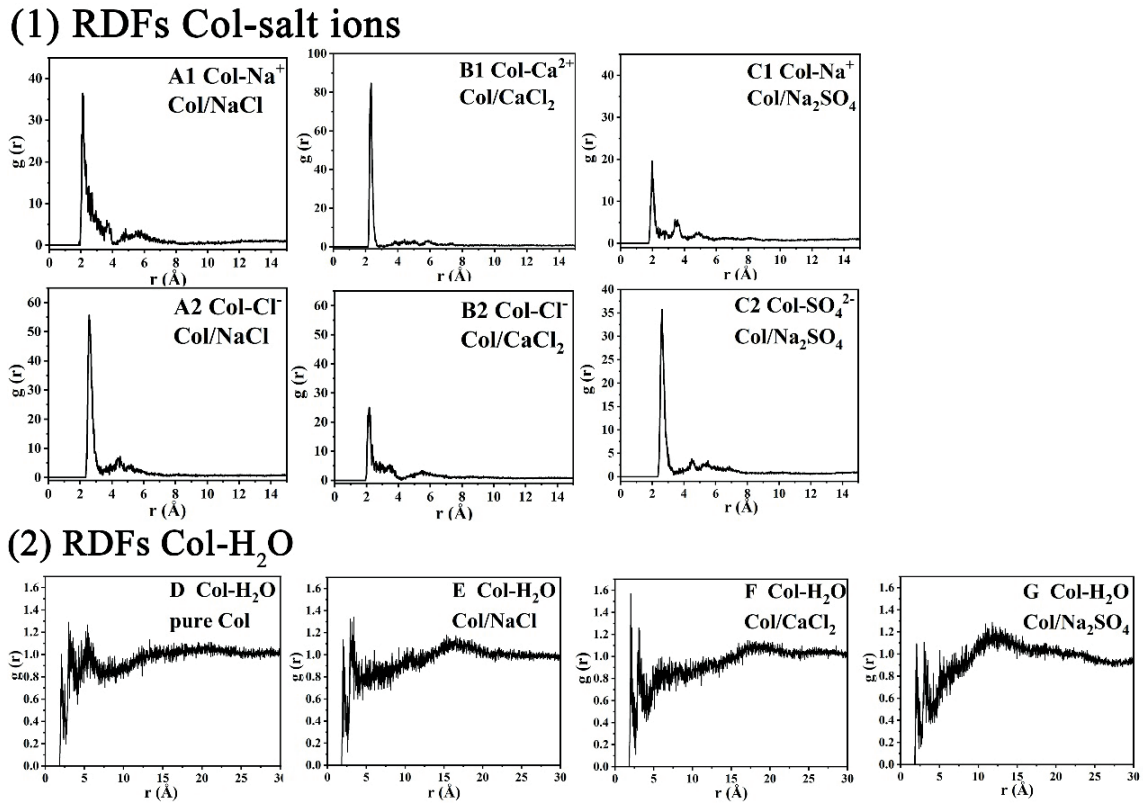

Figure 6. RDFs of collagen model with salt ions (**A1**–**C2**) and water (**D**–**G**) in different systems. **A1**, **A2**, **E**, [Col/NaCl] system; **B1**, **B2**, **F**, [Col/$CaCl_2$] system; **C1**, **C2**, **G**, [Col/Na_2SO_4] system; **D**, [pure Col] system.

to promote collagen aggregation and could induce collagen to form orderly aggregates with spaces, which could make water move outward. So when NaCl with high concentration was used in pickling, fibers would not be swollen and fiber bundles would be dispersed, which was beneficial for producing leather with good mechanical and hygienic performance.[2,5] Fibers and fiber bundles could be fully dispersed by $CaCl_2$, while fully dehydrated by Na_2SO_4, and moderately dispersed and dehydrated by NaCl.

Conclusion

The interaction mechanism between typical neutral salts (NaCl, $CaCl_2$, and Na_2SO_4) and collagen was investigated by combining experiments and MD simulation. The experimental results (Pyrene fluorescence spectra, DLS, AFM, and pI) indicated that the variation of the interaction between different neutral salts and collagen was accompanied with the changes in physicochemical properties of collagen. MD simulation further revealed that the electrostatic interactions of different salts with collagen molecules had the order of $CaCl_2$>Na_2SO_4>NaCl. Ca^{2+} of $CaCl_2$, SO_4^{2-} of Na_2SO_4, and Cl^- of NaCl were the contributing ions for the interactions of the salts with collagen. $CaCl_2$ tended to form intramolecular salt bridges with collagen and the binding of Ca^{2+} enhanced the electrostatic repulsions among collagen molecules, which led to the dispersing effect of $CaCl_2$. Na_2SO_4 tended to form intermolecular salt bridges between collagen molecules in the shape of agglomerates and the binding of SO_4^{2-} weakened the electrostatic repulsions, which promoted collagen interactions. NaCl was scattered around the collagen models, and its effect on collagen was much smaller. MD simulation with a natural collagen molecule model shed light on the mechanism between neutral salts and collagen at the molecular level. The results would provide guidance for further understanding and improving the use of neutral salts in the leather production.

Acknowledgement

This study was financially supported by the National Natural Science Foundation of China (No.22078206). The authors would thank to Zhonghui Wang (College of Biomass Science and Engineering, Sichuan University) for her help in AFM observations.

References

1. Covington, A. D.; Tanning chemistry: the science of leather, The royal society of chemistry, Cambridge, 166-620, 2011.
2. Li, X. X., Wang, Y. N., Li, J., et al.; Effect of Sodium Chloride on Structure of Collagen Fiber Network in Pickling and Tanning. JALCA **111**, 230-237, 2016.
3. Zhao, S. A., Zhang, M., Li, G. Y., et al.; Preparation and Characterization of Alkali-Soluble Collagen from Pigskin Shavings. JALCA **104**, 344-351, 2009.
4. Bulo, R. E., Siggel, L., Molnar, F., et al.; Modeling of bovine Type-I collagen fibrils: Interaction with pickling and retanning agents. *Macromol Biosci* **7**, 234-240, 2007.
5. Cheng, H. M., Chen, M., Li, Z. Q.; The Role of Neutral Salt for the Hydrolysis and Hierarchical Structure of Hide Fiber in Pickling. *JALCA* **109**, 125-130, 2014.
6. He, X., Ding, W., Zeng, Y. H., et al.; Insight into the Correlations Between Fiber Dispersion and Physical Properties of Chrome Tanned Leather. *JALCA* **115**, 23-29, 2020.
7. Lang, X. Y., Lyubovitsky, J. G.; Structural dependency of collagen fibers on ion types revealed by in situ second harmonic generation (SHG) imaging method. *Anal Methods-Uk* **7**, 1680-1690, 2015.
8. Zhang, X., Xu, S., Shen, L., et al.; Factors affecting thermal stability of collagen from the aspects of extraction, processing and modification. *Journal of Leather Science and Engineering* **2**, 2020.
9. Duan, L., Li, J. H., Li, C. H., et al.; Effects of NaCl on the rheological behavior of collagen solution. *Korea-Aust Rheol J* **25**, 137-144, 2013.
10. Li, Y. P., Douglas, E. P.; Effects of various salts on structural polymorphism of reconstituted type I collagen fibrils. *Colloid Surface B* **112**, 42-50, 2013.
11. Wang, L., Lyu, H., Zhang, X., et al.; Revealing the aggregation behaviors of mesostructured collagen by the evaluation of reconstituted collagen performance. *Food Hydrocolloid* **130**, 2022.
12. Wei, X. Y., Zhang, W. H., Shi, B.; Effect of Neutral Salt on Pickling and Tanning - A Study Based on Assembly Behaviour of Collagen. *J Soc Leath Tech Ch* **98**, 30-34, 2014.
13. Brown, E. M., Farrell, H. M., Wildermuth, R. J.; Influence of neutral salts on the hydrothermal stability of acid-soluble collagen. *J Protein Chem* **19**, 85-92, 2000.
14. KomsaPenkova, R., Koynova, R., Kostov, G., et al.; Thermal stability of calf skin collagen type I in salt solutions. *Bba-Protein Struct M* **1297**, 171-181, 1996.
15. Freudenberg, U., Behrens, S. H., Welzel, P. B., et al.; Electrostatic interactions modulate the conformation of collagen I. *Biophys J* **92**, 2108-19, 2007.

16. Sun, Q., Zeng, Y., Wang, Y. N., et al.; A deeper exploration of the relation between sulfonation degree and retanning performance of aromatic syntans. *Journal of Leather Science and Engineering* **3**, 2021.
17. Xu, Z. J., Yang, Y., Zhao, W. L., et al.; Molecular mechanisms for intrafibrillar collagen mineralization in skeletal tissues. *Biomaterials* **39**, 59-66, 2015.
18. Berg, A., Peter, C.; Simulating and analysing configurational landscapes of protein-protein contact formation. *Interface Focus* **9**, 2019.
19. Leo, L., Bridelli, M. G., Polverini, E.; Insight on collagen self-assembly mechanisms by coupling molecular dynamics and UV spectroscopy techniques. *Biophys Chem* **253**, 106224, 2019.
20. Niu, L. N., Jee, S. E., Jiao, K., et al.; Collagen intrafibrillar mineralization as a result of the balance between osmotic equilibrium and electroneutrality. *Nat Mater* **16**, 370-378, 2017.
21. Ding, Y. Q., Chen, C. L., Gu, Q. R., et al.; Application of molecular simulation to investigate chrome(III)-crosslinked collagen problems. *Model Simul Mater Sc* **22**, 2014.
22. Li, D., Yang, W., Li, G. Y.; Extraction of native collagen from limed bovine split wastes through improved pretreatment methods. *J Chem Technol Biot* **83**, 1041-1048, 2008.
23. Yang, H., Deng, Y., Xu, S. C., et al.; Investigation on the interaction of collagen molecules in solution with different acetic acid concentrations. *Journal of Applied Polymer Science* **134**, 2017.
24. Xu, S. C., Gu, M., Wu, K., et al.; Unraveling the interaction mechanism between collagen and alcohols with different chain lengths and hydroxyl positions. *Colloid Surface B* **199**, 2021.
25. Yan, M. Y., Li, B. F., Zhao, X.; Determination of critical aggregation concentration and aggregation number of acid-soluble collagen from walleye pollock (Theragra chalcogramma) skin using the fluorescence probe pyrene. *Food Chemistry* **122**, 1333-1337, 2010.
26. Tang, M., Li, T., Gandhi, N. S., et al.; Heterogeneous nanomechanical properties of type I collagen in longitudinal direction. *Biomech Model Mechan* **16**, 1023-1033, 2017.
27. Li, Y., Asadi, A., Monroe, M. R., et al.; pH effects on collagen fibrillogenesis in vitro: Electrostatic interactions and phosphate binding. *Materials Science and Engineering: C* **29**, 1643-1649, 2009.
28. Mertz, E. L., Leikin, S.; Interactions of inorganic phosphate and sulfate anions with collagen. *Biochemistry-Us* **43**, 14901-14912, 2004.
29. Tome, L. I. N., Jorge, M., Gomes, J. R. B., et al.; Toward an Understanding of the Aqueous Solubility of Amino Acids in the Presence of Salts: A Molecular Dynamics Simulation Study. *J Phys Chem B* **114**, 16450-16459, 2010.
30. Bensusan, H. B., Hoyt, B. L.; The Effect of Various Parameters on the Rate of Formation of Fibers from Collagen Solutions. *J Am Chem Soc* **80**, 719-724, 1958.
31. Oh, S., Nguyen, Q. D., Chung, K. H., et al.; Bundling of Collagen Fibrils Using Sodium Sulfate for Biomimetic Cell Culturing. *Acs Omega* **5**, 3444-3452, 2020.
32. Gao, M., Tian, Y., Zhang, X., et al.; A substrate protection approach to applying the calcium ion for improving the proteolysis resistance of the collagen. *Appl Microbiol Biotechnol* **105**, 9191-9209, 2021.
33. Zhang, Y., Liu, H., Tang, K., et al.; Effect of different ions in assisting protease to open the collagen fiber bundles in leather making. *Journal of Cleaner Production* **293**, 2021.

Region Wise Surface Level Defect Detection and Ranking of Crust Leather Images Based on Image Processing Techniques

by

S. Nithiyanantha Vasagam[a,b] and M. Sornam[a*]

[a]*Department of Computer Science, University of Madras, Guindy Campus,* Chennai – 600025, Tamil Nadu, India

[b]*Knowledge Portfolio Management Department, Council of Scientific & Industrial Research (CSIR) - Central Leather Research Institute (CLRI),* Adyar, Chennai – 600020, Tamil Nadu, India

Abstract

Sorting and aligning of crust leather for grading on position wise defect distribution is one of the methods adopted in the tanning industry. This method is generally carried out manually by a veteran on official sampling position and their input is critical because it is directly linked to sales of the crust leather. The opinion of the experts is believed to be stable and consumes a good amount of time too. Hence, in the current research a robust defect detection method and ranking of crust leather images based on image processing techniques is proposed to give a stable solution in a short span of time. A custom-made dataset of crust leather images consisting of 5640 images were used in this study. The pixel intensity has been extracted on demarcated position of various regions including neck, belly left, belly right, center and butt instead of official sampling position through horizontal and vertical mapping of coordinates with a new method Grading Score on Image Position wise (GSIP) on the actual images. The image processing techniques using Canny Edge Detection and filters such as Laplacian, Median, Prewitt, Roberts, Sobel and Scharr were implemented to get the pixel intensity grouped and classified based on parameters within acceptable range using a Naïve Bayes Classifier. The classifier confirms that the accuracy of Set I - Actual Images and Set II - Defects with implementation of canny edge detection over other image processing techniques at 99.50%. Therefore, the current research confirms that the proposed GSIP method would give an additional tool to inspectors while ranking the crust leather based on region wise surface level defect detection of crust leather images based on image processing techniques.

Introduction

Leather is a by-product of the meat industry and annually the international trade is estimated to be about US$ 80 billion.[1] The conventional process associated in making leather starts from the initial stage of collection of raw hides & skins, then soaking, liming, fiber opening (re-liming), fleshing, deliming, pickling, chrome tanning, splitting & shaving, post tanning (crust leather)[2] and ends up with the stage called finishing.[3] Finished leather is further processed for the making of leather footwear, leather garments, leather goods and saddlery & harness. The value of the finished leather is determined depending upon the observations[4] made on the surface on official sampling positions of the crust leather. The role of inspectors is to observe the surface level[5] and it is the key which basically determines the value of the finished leather. Experts usually segregate upon the ranking like 1, 2, 3, 4, 5, 6, 7 and R. Normally, the rank 1-2 will go into high-end products, 3-4 will go into mid-range products and 5-6 will go for low range products and the R will be considered for direct rejection.[6,7]

To extract some useful information, the image processing technique is applied on an image with Edge Detection and Filters. Yang Liu et al.[8] has presented an adaptive, robust and effective edge detector and described edge points as strong edge, pixels, weak edge pixels and non-edge pixels depend on the gradients while segmentation with Canny algorithm. Gandhi et al.[9] applied Canny edge detection on images of letters placed on ground and captured through drone cameras. The Canny edge detector[10] goes a step further by employing non-maximum suppression to extract a thinner contour and applying the double threshold algorithm to get the weak edges. However, it is difficult to get a suitable threshold, especially in a dynamic environment where the background changes rapidly. To extract the structural details Canny edge detection[11] technique is applied based on double threshold algorithm to extract a thinner contour even on the weak edges in all real edges which is shown in Equation 1.

$$\blacktriangledown (Ga * Im) \text{ where Ga: Gaussian and Im: Image} \quad (1)$$

Filters such as Laplacian, Median, Sobel, Roberts, Scharr and Prewitt detect pixels with brightness, colors and gradients to reduce noise.[12] Laplacian enhances the edges of an image with pixel intensity values. Median filter reduces noise in an image based on pixel intensities. The Sobel calculates the gradient of image intensity on regions of high spatial level of each pixel. Roberts detect the edge of the image. Scharr detects edges deriving by pixel intensity corresponding to gradient edges. Prewitt detects edges based on the pixel intensities of an image in horizontal and vertical directions.

Aslam, M., et al.[13] have reported on inspection methods based on leather surface defects based on deep learning methods. They have mentioned that the market value will be reduced based on significant defects present in raw hides and leather as per the sub-divisions of a hide such as Head, Shoulder, Bend, Belly, Side, Crop,

*Corresponding author email: madasamy.sornam@gmail.com

Manuscript received February 20, 2022, accepted for publication February 27, 2023.

Back, Croupon, Dosset and Culatta. Lai, K., et al.[14] have presented an automated vision system intending to detect and classify surface defects in steel plate. Authors implemented Sobel filter for detecting edges and adopted fuzzy neural network for the defect classification.

Gong, R., et al.[15] have proposed a classifier support vector hyper-spheres with insensitivity to noise (INSVHs) on steel plate surface defects such as hole, scratch, bruise, wave, scarring and scale based on region of defects. Hu, L., et al.[16] have developed a new method to identify steel-plate surface defects such as Common defects consisting of Bumps, Scratches & Oil Spots and non-common defects consisting of Stains & Dirtiness. They have implemented synthetic minority over-sampling technique (SMOTE) and AdaBoost.BK algorithm.

Suvdaa, B., et al.[17] have proposed a framework for exact defect points by forming a single image on the basis of feature vectors in steel surface using Scale Invariant Feature Transform for defects detection and Support Vector Machines for defects classification. Villar, P., et al.[18] have proposed an automatic method for defect classification of the Wet Blue leather from the Gray Scale image, the RGB and HSV color model. The features were extracted based on the Sequential Forward Selection method and classification was implemented using a Supervised Neural Network.

Pistori, H., et al.[19] have suggested defect detection in raw hide and wet blue leather having four different defects such as brand marks, tick marks, cuts and scabies through demerit count reference standard for leather raw hides. They have implemented two tailed, t-student test while classification using support vector machines. Vasagam, S.N., et al.[20] have presented the options of defects Identification of Crust Leathers using Computer-aided Grading by calculating position of defects, extent of defects and the distribution of defects with a Logical table for objective grading.

Liong, S.T., et al.[21] have proposed instance segmentation to distinguish whether the leather sample contains a defective part or not using deep learning to classify the three-categories of leather images. Jian, L., et al.[22] have proposed using Feed-forward Neural Network (FNN) by combining decision trees in defect detection and classify the leather based on surface defects of shape, texture and color. Bong, H.Q., et al.[23] has introduced an automated vision-based system which consists of an image grabbing mechanism on locating position of the leather defects by classifying based on color, shape and texture using the classifier SVM.

Sornam, M. and Vasagam, S.N.[24] had suggested a model to group the Intermittent Leather Images using Linear Discriminant Model as per the category of normal leather and defective leather based on surface level features such as base color, other than base color, share of regions, share of cutting area, share of cutting value, position wise length and position wise breadth. Xie, X., et al.[25] has proposed an improved image matching algorithm of defects by describing spatial signals on navel orange surface based on compressed sensing by combining of wavelet transform (WT) and speeded up robust features (SURF).

Aslam, Y., et al.[26] has proposed an automatic segmentation and quantification approach for inspecting defects on Metal from digital images consisting of input image and ground truth using convolutional neural network (CNN) approach. Vasagam, S.N. and Sornam, M.[27] has proposed an Intermittent Leather Defect Detection based on Outer and Inner radius using Leather Image Surface Feature Extraction LISFE derived from Black Hat transformation

Table I

Summary of Authors, Techniques and Area

S. No	Authors	Name of the Technique/method	Area / Material
1.	Aslam, M., et al.[13]	Deep Learning Methods	Wet blue leather
2.	Lai, K., et al.[14]	Automated Vision System	Steel
3.	Gong, R., et al.[15]	Support Vector Hyper-Spheres with Insensitivity to Noise	Steel
4.	Hu, L., et al.[16]	New method to identify steel-plate surface defect	Steel
5.	Suvdaa, B., et al.[17]	Scale Invariant Feature Transform and Support Vector Machines	Steel
6.	Villar, P., et al.[18]	Sequential Forward Selection method and Supervised Neural Network	Wet Blue leather
7.	Pistori, H., et al.[19]	Sequential Forward Selection and Supervised Neural Network	Raw hide and wet blue leather
8.	Vasagam, S.N., et al.[20]	Computer Aided Grading	Crust Leather
9.	Liong, S.T., et al.[21]	Instance segmentation	Leather
10.	Jian, L., et al.[22]	Feed-forward Neural Network	Leather
11.	Bong, H.Q., et al.[23]	Support Vector Machines	Leather
12.	Sornam, M. and Vasagam, S.N.,[24]	Linear Discriminant Model	Intermittent Leather
13.	Xie, X., et al.[25]	Wavelet Transform and Speeded Up Robust Features	Orange
14.	Aslam, Y., et al.[26]	Convolutional Neural Network	Metal
15.	Vasagam, S.N. and Sornam, M.,[27]	Ensemble Algorithms	Intermittent Leather

and Hough transformation. The majority of the research discussed as shown in Table I in this field had explored classifying the images on the basis of surface level. It shows the importance of studying the images on the surface and indicates that there exists an ample scope in determining the surface level defect detection on region wise on crust leather images based on image processing techniques.

- The authors in the research article have set an objective to give emphasis on region wise surface level defect detection instead of official sampling position and then ranking of the leather images on the basis of position of the region using image processing techniques. The contributions of authors are given below.
- A custom-made dataset of crust leather images consisting of 5640 images consisting of two datasets. Dataset I consists of the original images with truth values, original images applied with Canny Edge Detection and also from Filters such as Laplacian, Median, Prewitt, Roberts, Sobel and Scharr. Dataset II consists of original images with truth values and original images applied with Canny Edge Detection.
- Pixel intensity has been extracted on five regions based on Horizontal and Vertical mapping of coordinates.
- Ranking of crust leather image has been implemented from the extracted feature with the proposed method called Grading Score on Image Position wise (GSIP).
- Classification of ranking by grouping them as "within the acceptable Range" or "Not within the acceptable Range" based on the threshold value set as the individual rank which is less than or equal to threshold value of four with Naïve Bayes classifier.

The manuscript has covered the remaining sections of Methodology, Results & Discussions in the following sections which is represented in Figure 1 and working model is shown in Figure 2.

1. Creation of Dataset I and II
2. Implementation of contour of five regions and applied Canny Edge Detection & Other Filters
3. Feature extracted based on Horizontal and Vertical mapping of coordinates
4. Generation of Ranking Matrix of crust leather image from the extracted feature with the proposed method called Grading Score on Image Position wise (GSIP)
5. Classification of ranking by grouping them as "within the acceptable Range" or "Not within the acceptable Range" based on Naïve Bayes Classifier.

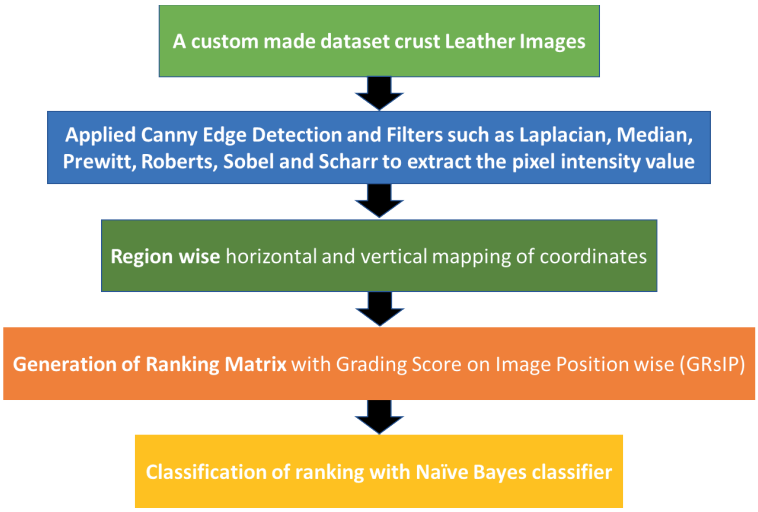

Figure 1. Workflow

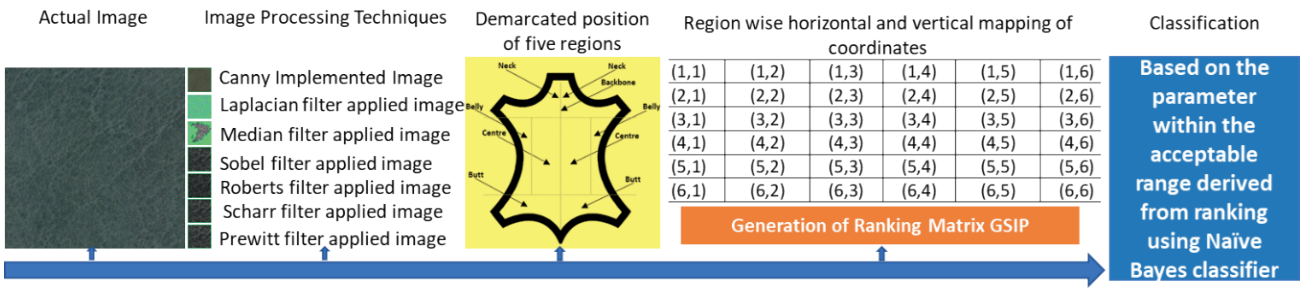

Figure 2. Working Model

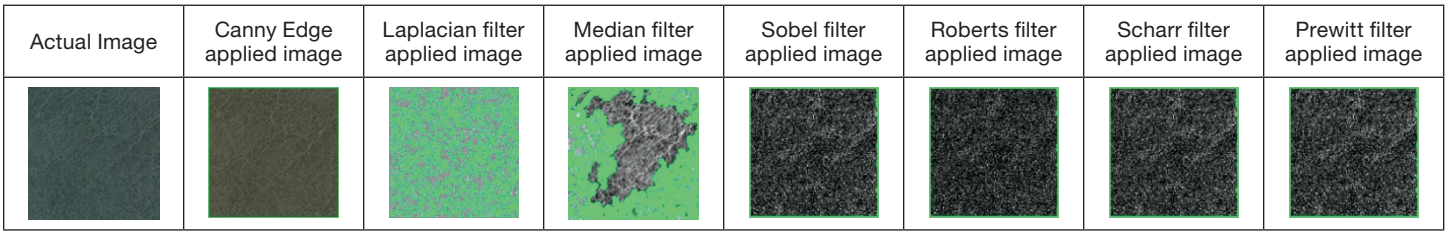

Figure 3. Sample image and filtered images Workflow

Methodology

A. **Dataset of Crust leather images:** Image dataset of Crust leather images in the Set I and Set II consisted of 4872 and 768 respectively. These images were originally taken using a Konica camera and cropped into the size of 250 x 250 with 72 dpi for Set I and 300 x 300 with 96 dpi for Set II. In the Set I image, dataset is consisting of image filtered from actual images from filters such as Laplacian, Median, Sobel, Roberts, Scharr and Prewitt as shown in Figure 3.

B. **Region wise Horizontal and Vertical Mapping - Feature Extraction:** In general, the experts who do the sorting will look into the areas of official sampling position and cutting area consisting of the Neck, Belly, and, Butt positions in the hide/skin.[28] The region of interest of the sorting person is mostly depending on the official sampling position on the hide or skin. Gogaev, O.K. and Demurova, A.R.,[29] had studied on thickness on the belly region and also mentioned about other regions such as neck, shoulder and thigh. Dagnew, N., et al.[30] studied differences between Butt, Neck and Belly Regions while making an assessment of histology and biochemical properties of sheep skin. Basil-Jones, M.M., et al.[31] measured edge-on the three positions namely Belly, official sampling position and, neck. In line with this, the current study has introduced a new method for defect detection on the five positions of the hide/skin namely Neck (N), Belly Left (BL), Belly Right (BR), Centre (C) and Butt (BT). The conventional sampling method is shown in Figure 4a and the proposed surface-based sampling is shown in Figure 4b.

Every pixel in each and every region was applied with binary threshold in identifying the boundaries of the particular shape which is otherwise called contours and stores the coordinates of row and column. Accordingly, the Class Label (C_i) for horizontal (Row_i) and vertical ($Column_j$) is calculated as shown in the Equation 2.

$$C_{ij} = (Row_i, Column_j \quad (2)$$

where C_i: Image Cropping in line with co-ordinates of i^{th} row and j^{th} column

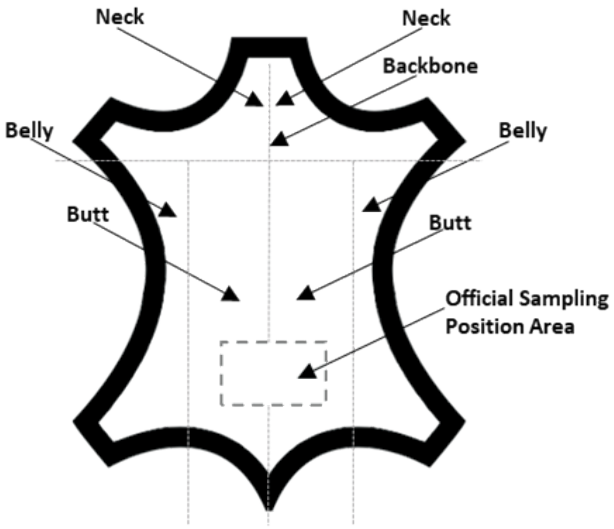

Figure 4a. Demarcated position of various regions within the hide for official sampling position

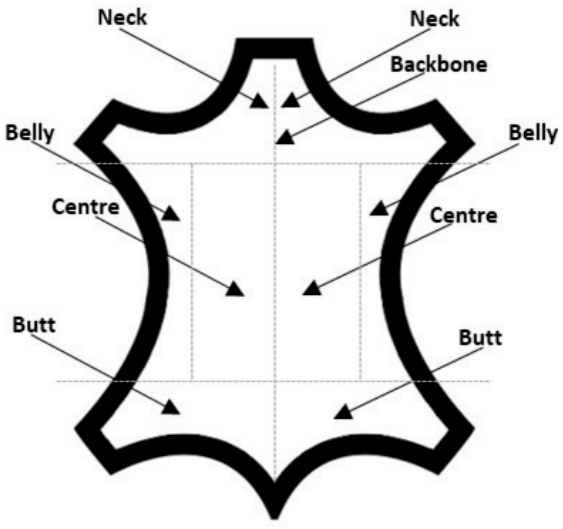

Figure 4b. Demarcated position of various regions within the hide for surface defect detection

Table I

Sample 6×6 Matrix representation of pixel points where i is row, j is column and n represent the size = 6

(1.1)	(1.2)	(1.3)	(1.4)	(1.5)	(1.6)
(2.1)	(2.2)	(2.3)	(2.4)	(2.5)	(2.6)
(3.1)	(3.2)	(3.3)	(3.4)	(3.5)	(3.6)
(4.1)	(4.2)	(4.3)	(4.4)	(4.5)	(4.6)
(5.1)	(5.2)	(5.3)	(5.4)	(5.5)	(5.6)
(6.1)	(6.2)	(6.3)	(6.4)	(6.5)	(6.6)

Table II

Representation of three region mapping of pixel point as Row Size (RS) = n/3

Region 1	Region 2	Region 3
Where i=1, j=1	Where i=RS, j=1	Where i=RS * 2, j=1
Row count start = i	Row count start = i	Row count start = i
Row cound end = RS	Row cound end = RS * 2	Row cound end = j
Column Count Start = i	Column Count Start = j	Column Count Start = j
Column Count end = j	Column Count end = n	Column Count end = n

The mapping of pixel points at each and every region is designed as shown in Table I and Table II for three regions. The image cropping is implemented for the Region 1, the i^{th} and j^{th} values are equal as it becomes the starting point, for the Region 2, i^{th} value becomes row size and j^{th} value as 1 as this is the mid-point and for the Region 3, the i^{th} value becomes row size multiplied by 2 and j^{th} value as 1 becomes last point.

Generation of Ranking Matrix:

In generation of ranking, the label values of Horizontal and vertical class values are mapped with the possible probabilities which is derived from the threshold value of the image. The cutting area is about 87.88% and as per the grading mentioned in the Table III, it fits in the grade 4.

Yeh et al.,[32] had suggested methods are contrast method through histogram, internal color level method, external color level method and fuzzy method is by establishing a demerit count between physical unusable area calculation and unusable region defect grouping based on the percentage share of unusable area. However, they have commented that there is no stable method and for classifying the wet blue hide have been done using the Table IV. As per the table, if the area is above 8750 pixels, the grade will be allotted as 4. Establishing a Demerit Count Reference Standard[33] for the Classification and Grading of Leather Hides.

Table III

Cutting area and corresponding Grading

Grade	Cutting Area
1	100 %
2	95%
3	90%
4	85%
5	80%
6	70%
R	<70%

Table IV

Intermittent Leather grading based on area of usefulness based on demerit count

Grade or Rank	Area of usefulness
1	<2500
2	2500 to <5000
3	5000 to < 8750
4	>= 8750

Algorithm I : Rank Calculation:

Step 1: Input ClassLabelHor, ClassLabelVer

Step 2: if ClassLabelHor and ClassLabelVer are same then ClassRank = either ClassLabelHor nor ClassLabelVer

Step 3: otherwise ClassRank will be maximum value of either ClassLabelHor nor ClassLabelVer

Label values of ClassLabelHor, and ClassLabelVer are derived based on the pixel intensity value associated with respect of the co-ordinates of horizontal (Row_i) and vertical ($Column_j$) as stated in Table V.

Grading Score on Image Position wise (GSIP) ranking the Crust leather image based on the Algorithm I. The ClassRank value is carried with the input value of Horizontal and Vertical as per the equation (3) and (4). GSIP is predominately considering the useful area present in the Center region. Accordingly, based on the possible probabilities of the N, BL, BR, C and BT, RankClass Label is created with the ranking such as 1, 2, 3, 4, 5, 6, 7 and 8.

$$\text{ClassLabelHor} = I < 2 \text{ where I is the intensity value} \quad (3)$$

$$\text{ClassLabelVer} = J < 5 \text{ where J is the intensity value} \quad (4)$$

Where I and J is represents P(N), P(BR), P(BR), P(C), P(BT), P(N), P(BR), P(BR), P(C), P(BT) which are Pixel intensity value of Neck, Belly Left, Belly Right, Centre and Butt respectively.

Table V

Ranking based on Pixel intensity value associated with the co-ordinates of horizontal (Row_i) and vertical ($Column_j$)

P(N) <=2 for horizontal <=5 for vertical	P(BL) <=2 for horizontal <=5 for vertical	P(C) <=2 for horizontal <=5 for vertical	P(BL) <= 2 for horizontal <=5 for vertical	P(BR) <= 2 for horizontal <=5 for vertical	ClassLabelHor / ClassLabelVer
Yes	Yes	Yes	Yes	Yes	1
Yes	Yes	Yes	Yes	No	2
Yes	Yes	Yes	No	Yes	2
Yes	Yes	Yes	No	No	3
Yes	No	Yes	Yes	Yes	2
Yes	No	Yes	Yes	No	3
Yes	No	Yes	No	Yes	3
Yes	Yes	Yes	No	No	4
No	Yes	Yes	Yes	Yes	2
No	Yes	Yes	Yes	No	3
No	Yes	Yes	No	Yes	3
No	Yes	Yes	No	No	4
No	No	Yes	Yes	Yes	3
No	No	Yes	Yes	No	4
No	No	Yes	No	Yes	4
No	No	Yes	No	No	5
Yes	Yes	No	Yes	Yes	6
Yes	Yes	No	Yes	No	7
Yes	Yes	No	No	Yes	7
Yes	Yes	No	No	No	8
Yes	No	No	No	No	8
Yes	No	No	Yes	Yes	6
No	Yes	No	Yes	Yes	7
No	No	No	No	No	8

Classification with Naive Bayes:

Shi, Y., et al.[34] had proposed a jamming identification scheme based on small data driven Naive Bayes classifier. For the classification using Naive Bayes classifier, the ranks are grouped into two cases, the first case as "within the acceptable Range" having the value less than or equal to 4 and the alternative case having the value more than 8 as "Not within the acceptable Range" corresponding to an image.

Results & Discussions

Initially the original crust image of Set I are applied with Canny Edge Detection and also filtered with Filters such as Laplacian, Median, Prewitt, Roberts, Sobel, Scharr. After which as stated in Table VI, the Contour of the images are identified on the five positions consisting of Neck, Belly Right, Belly Left, Butt and Center. Then each and every image is broken into five parts as per the anatomy of the animal to identify the Contour of five regions based on the horizontal and vertical coordinates.

Table VI

Coordinates for an image of 250 × 250

Region / Area	Row	Column	Height	Width
Neck	1	1	10	250
Belly Left side	1	11	200	50
Centre	50	11	200	150
Butt	1	211	40	250
Belly Right side	201	11	200	50

Table VII

Demarcated position of various regions within the hide for surface defect detection

Actual Image	Neck region	Belly Left side region	Centre region	Butt region	Belly Right side region
 (A)					
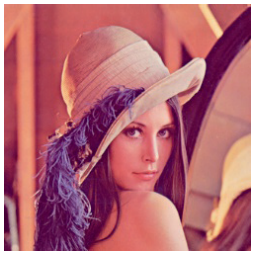 (B)			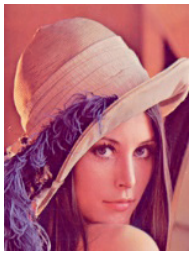		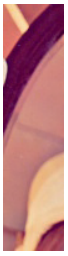
 (C)					
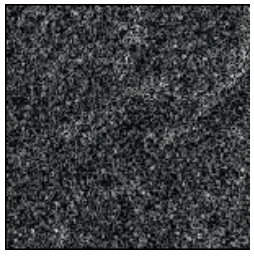 (D)					

Img	count_no_N	rowwisecount_N	count_no_BT	rowwisecount_BT	count_no_C	rowwisecount_C	count_no_BL	rowwisecount_BL	count_no_BR	rowwisecount_BR	ClassLabelHor	ClassLabelVer
1	2	37	1	5	1	37	1	5	1	5	1	7
2	1	5	1	5	1	5	1	5	1	5	1	1
3	1	5	1	5	1	5	1	5	1	5	1	1
4	1	5	1	5	1	5	1	5	1	5	1	1
5	5	36	3	5	1	260	1	140	2	82	3	8
6	1	40	1	117	1	57	1	85	1	18	1	8
7	8	57	1	224	1	249	1	110	1	92	2	8
8	3	5	1	73	1	64	2	153	1	45	2	8
9	1	5	1	5	1	25	1	42	2	25	1	8
10	1	5	1	27	1	5	1	62	1	5	1	3
11	1	5	1	5	1	20	1	5	1	5	1	6
12	2	9	1	18	1	12	1	10	1	5	1	8
13	1	5	1	18	1	5	1	5	1	5	1	2
14	1	5	1	5	1	5	1	5	1	5	1	1
15	1	5	3	277	4	122	4	156	1	33	8	8
16	1	5	1	14	1	5	1	10	1	5	1	3
17	1	5	1	5	1	5	1	5	1	5	1	1
18	2	17	2	90	3	20	1	13	1	63	6	8

Figure 5. output derived from the Algorithm I

The sample images of (A) Camera Man, (B) Leena, (C) Hide image and (D) Prewitt Filtered image are given in the table VII as per the demarcated position of various regions consisting of Neck region, Belly Left side region, Centre region, Butt region, and Belly Right side region.

The table VIII shows the Probabilities and various Position with Ranking Matrix of Dataset I and II generated from Algorithm I whereas initially the ranking is generated for Dataset I and it is observed from the Table VIII that the canny implemented Set I - Actual Images Applied with Canny confirms significantly working well over other dataset I filters with the Set I - Actual Images with Truth Values. Hence, in the dataset II, only the Canny edge detection is implemented and it also confirms significantly that out of 384 defect-based images to an extend of maximum. Once again it is confirming that the Canny edge detection-based filtering is significantly working well. A sample of the output is shown in Figure 5 Position with Ranking Matrix for the corresponding column and row of regions.

The Ranking of Dataset I and II are grouped into two categories namely within the acceptable range and not in the acceptable range which is derived from the ClassRank having less than 5. The GSIP is applied on the identified dataset is shown in Figure 6. According to the chosen dataset, the rank 8 covers maximum. The result shows that the defect classification with respect to Set I- Actual Images, Set I- Actual Images with Canny are better than of Set I – Laplacian Filter applied in Actual Image, Set I – Median Filter applied in Actual Image, Set I – Prewitt Filter applied in Actual Image, Set I – Roberts Filter applied in Actual Image, Set I – Sobel Filter applied in Actual

Table VIII

Ranking of Dataset I and II

Data Set I & II / Ranking	Rank 1	Rank 2	Rank 3	Rank 4	Rank 5	Rank 6	Rank 7	Rank 8
Set I - Actual Images with Truth Values	564	33	1	0	0	9	2	0
Set I - Actual Images Applied with Canny	0	0	92	504	4	1	0	8
Set I – Laplacian Filter Applied in Actual Image	54	6	3	1	1	4	0	540
Set I – Median Filter Applied in Actual Image	23	21	3	0	1	4	0	557
Set I – Prewitt Filter Applied in Actual Image	34	12	11	1	5	7	4	535
Set I – Roberts Filter Applied in Actual Image	51	10	7	2	1	6	4	528
Set I – Sobel Filter Applied in Actual Image	35	14	11	5	3	4	4	533
Set I – Scharr Filter Applied In Actual Image	39	10	7	2	2	5	1	543
Set -II - Defects Truth Values	37	16	7	1	1	5	3	314
Set -II - Defects Canny	0	1	0	0	0	0	0	383

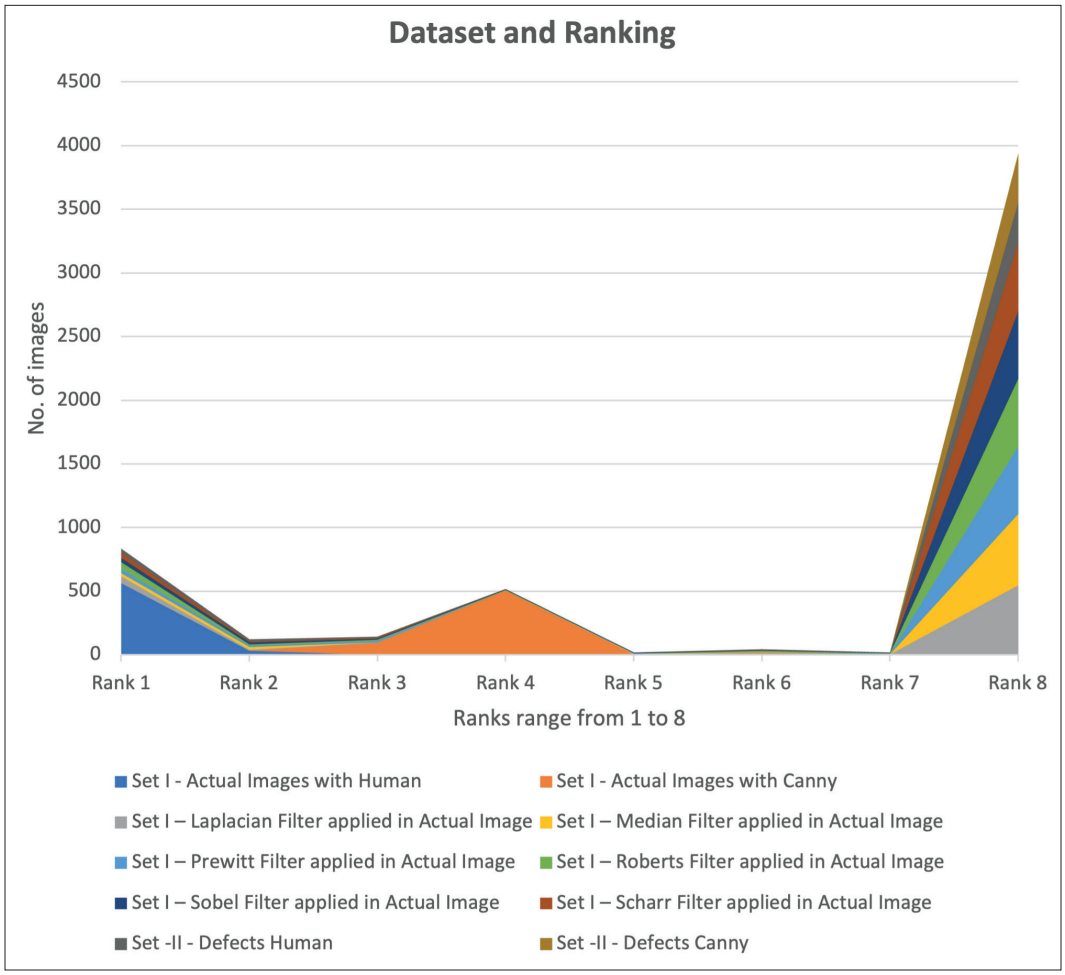

Figure 6. The GSIP chart of the dataset I and II

Table IX

Naïve Bayes Classifier Comparison of various image files

Dataset	Within acceptable range	Not within the acceptable range	Classification Accuracy
Set I - Actual Images with Human	598	11	0.99
Set I - Actual Images with Canny	596	13	**0.995**
Set I – Laplacian Filter applied in Actual Image	64	545	1
Set I – Median Filter applied in Actual Image	47	562	1
Set I – Prewitt Filter applied in Actual Image	58	551	0.985
Set I – Roberts Filter applied in Actual Image	70	539	0.99
Set I – Sobel Filter applied in Actual Image	65	544	0.99
Set I – Scharr Filter applied in Actual Image	58	551	0.99
Set -II - Defects Human	61	323	0.945
Set -II - Defects Canny	1	383	**0.995**

Image and Set I – Scharr Filter applied in Actual Image. In the case of Set II, classification of Set II – Actual Images and Set II – Actual Images with Defect implemented Canny.

Comparison of Naïve Bayes Classifier is shown in Table IX confirming the significant accuracy of Set I - Actual Images and Set II - Defects with implementation of canny edge detection over other image processing techniques at 99.50%. Moreover, among the filters applied in Set I, the sobel filter is also performing better than other filters at 91.17%. Hence, current study confirms that the proposed GSIP based ranking in detecting the surface based defect is significant as per the demarcated position of five regions within the hide for surface defect detection.

Conclusion

The proposed ranking matrix on the basis of demarcated position of five regions within the hide for surface defect detection namely Neck, Belly Left, Belly Right, Center, and Butt using Grading Score on Image Position wise (GSIP) is significantly performing as the accuracy of Set I - Actual Images and Set -II - Defects with implementation of canny edge detection over other image processing techniques at 99.50% for the dataset consisting of 5640 images using Naïve Bayes Classifier in this research article. Hence, current study confirms that the demarcated position of five regions and ranking would give an additional tool to inspectors while ranking the Crust leather.

Acknowledgments

Authors are thankful to University of Madras, Chennai and CSIR-Central Leather Research Institute (CSIR-CLRI), Chennai. The authors also sincerely acknowledging the support extended from Tanners Association and using of figures of CAMERA MAN and LEENA. The authors also acknowledge the CSIR-CLRI communication No. 1685.

References

1. International Trade Centre (ITC), Geneva, Switzerland, (https://www.intracen.org/itc/sectors/leather/)
2. Covington, A.D. and Wise, W.R.; Current trends in leather science. *Journal of Leather Science and Engineering*, **2**(1), pp.1-9, 2020.
3. Sathish, M., Aravindhan, R. and Rao, J.R.; Salt-free Chromium Tanning: Practical Approaches. *JALCA* **117**(1), pp.3-9, 2022.
4. Muthukrishnan, M., Jaimohan, S., Naresh, M.D., Ramesh, R. and Aravindhan, R.; A Non-destructive Evaluation of Fluffiness of Leather. *JALCA* **112**(08), pp.263-269, 2017.
5. Cooper, R.G.; Ostrich (Struthio camelus var. domesticus) skin and leather: A review focused on southern Africa. *World's Poultry Science Journal*, **57**(2), pp.157-178, 2001.
6. Gore, S.E., Laing, R.M., Lange, S., Scobie, D.R. and Young, S.R.; Changes to surface flaws on deer hides during processing to garment leather. *Journal of the Society of Leather Technologists and Chemists,* **86**(5), pp.183-7, 2002.
7. Gan, Y.S., Chee, SS., Huang, YC. et al.; Automated leather defect inspection using statistical approach on image intensity. *J Ambient Intell Human Comput* **12**, 9269–9285 (2021). https://doi.org/10.1007/s12652-020-02631-6
8. Liu, Y., Xie, Z., & Liu, H.; An adaptive and robust edge detection method based on edge proportion statistics. *IEEE Transactions on Image Processing*, **29**, 5206-5215, 2020.
9. Gandhi, M., Kamdar, J., & Shah, M.; Pre-processing of non-symmetrical images for edge detection. *Augmented Human Research*, **5**(1), 1-10, 2020.
10. Zhikang Xiao, Yang Zou, and Zhen Wang; An improved dynamic double threshold Canny edge detection algorithm, Proc. SPIE 11430, MIPPR 2019: Pattern Recognition and Computer Vision, 1143016 (14 February 2020); https://doi.org/10.1117/12.2539300
11. Li, B., He, F. and Zeng, X.; A novel privacy-preserving outsourcing computation scheme for Canny edge detection. The Visual Computer, pp.1-19, 2021.
12. Kumar, A.A., Lal, N. and Kumar, R.N.; A Comparative Study of Various Filtering Techniques. In 2021 5th International Conference on Trends in Electronics and Informatics (ICOEI), 26-31, IEEE. June 2021,
13. Aslam, M., Khan, T.M., Naqvi, S.S., Holmes, G. and Naffa, R., On the application of automated machine vision for leather defect inspection and grading: A survey. IEEE Access, **7**, 176065-176086, 2019.
14. Lai, K., Zhang, H. and Dai, D.; New approach to classification of surface defects in steel plate based on fuzzy neural networks. In Optical Information Processing Technology **4929**, 447-456. International Society for Optics and Photonics. September 2002.
15. Gong, R., Chu, M., Yang, Y. and Feng, Y.; A multi-class classifier based on support vector hyper-spheres for steel plate surface defects. *Chemometrics and Intelligent Laboratory Systems*, **188**, 70-78, 2019.
16. Hu, L., Zhou, M., Xiang, F. and Feng, Q.; Modeling and recognition of steel-plate surface defects based on a new backward boosting algorithm. The International *Journal of Advanced Manufacturing Technology*, **94**(9), 4317-4328, 2018.
17. Suvdaa, B., Ahn, J. and Ko, J.; Steel surface defects detection and classification using SIFT and voting strategy. *International Journal of Software Engineering and Its Applications*, **6**(2), 161-166, 2012.
18. Villar, P., Mora, M. and Gonzalez, P.; A new approach for wet blue leather defect segmentation. In Iberoamerican Congress on Pattern Recognition 591-598, Springer, Berlin, Heidelberg, November 2011.
19. Pistori, H., Paraguassu, W.A., Martins, P.S., Conti, M.P., Pereira, M.A. and Jacinto, M.A.; Defect detection in raw hide and wet blue leather. *In Proc. Int. Symp. CompIMAGE,* 355, May 2018.
20. Vasagam, S.N., Madhan, B., Chandrasekaran, B. and Rao, J.R.; 2013. Studies on Selective Defect Identification of Crust Leathers for Computer-aided Grading. *JALCA*, **108**(06), 210-220, 2013.

21. Liong, S.T., Zheng, D., Huang, Y.C. and Gan, Y.S.; Leather defect classification and segmentation using deep learning architecture. *International Journal of Computer Integrated Manufacturing*, 33(10-11), pp.1105-1117, 2020.
22. Jian, L., Wei, H. and Bin, H.; June. Research on inspection and classification of leather surface defects based on neural network and decision tree. In 2010 International Conference On Computer Design and Applications, 2, V2-381, IEEE, June 2010.
23. Bong, H.Q., Truong, Q.B., Nguyen, H.C. and Nguyen, M.T.; Vision-based inspection system for leather surface defect detection and classification. In 2018 5th NAFOSTED Conference on Information and Computer Science (NICS) 300-304, IEEE. November 2018.
24. Sornam, M. and Vasagam, S.N.; Surface Defect Identification and Grouping of Intermittent Leather Images using Linear Discriminant Model. *International Journal of Innovative Technology and Exploring Engineering*, **8**(12), 2253-2259, 2019.
25. Xie, X., Ge, S., Xie, M., Hu, F., Jiang, N., Cai, T. and Li, B.; Image matching algorithm of defects on navel orange surface based on compressed sensing. *Journal of Ambient Intelligence and Humanized Computing*, 1-9, 2018.
26. Aslam, Y., Santhi, N., Ramasamy, N. and Ramar, K.; Localization and segmentation of metal cracks using deep learning. *Journal of Ambient Intelligence and Humanized Computing,* 1-9, 2020.
27. Vasagam, S.N. and Sornam, M.; Intermittent Leather Defect Detection Based on Ensemble Algorithms Derived from Black Hat Transformation and Hough Transformation. *In ICT Analysis and Applications*, 35-45, Springer, Singapore, 2022.
28. 18 Covington, A.D.; Tanning chemistry: The Science of Leather. Royal Society of Chemistry, 2009.
29. 19 Gogaev, O.K. and Demurova, A.R.; Topographic features of sheep skin and coat structure. *Journal of Livestock Science* (ISSN online 2277-6214), **12**, 141-146, 2021.
30. Dagnew, N., Punitha, V., Sreeram, K.J., Rao, J.R. and Nair, B.U.; An Assessment of Differences between Butt and Belly Regions of Indian Sheep Skin. *JALCA*, **110**(06), pp.165-176, 2015.
31. Basil-Jones, M.M., Edmonds, R.L., Cooper, S.M., Kirby, N., Hawley, A. and Haverkamp, R.G.; Collagen fibril orientation and tear strength across ovine skins. *Journal of Agricultural and Food Chemistry*, **61**(50), 12327-12332, 2013.
32. S. Yeh C. and Perng D.; A Reference Standard of Defect Compensation for Leather Transactions. *The International Journal of Advanced Manufacturing Technology*, 1197 – 1204, 2005.
33. Yeh C. and Perng D. B.; Establishing A Demerit Count Reference Standard for the Classification and Grading of Leather Hides. *The International Journal of Advanced Manufacturing Technology*, **18**(10):731–738, 2001.
34. 22 Shi, Y., Lu, X., Niu, Y. and Li, Y., 2021. Efficient Jamming Identification in Wireless Communication: Using Small Sample Data Driven Naive Bayes Classifier. IEEE Wireless Communications Letters.

Isolation and Identification of Moderately Halophilic Bacteria from Soak Liquor Samples Collected of Leather Tanneries

by
P. Caglayan[1]*
[1]*Division of Plant Diseases and Microbiology, Department of Biology, Faculty of Science, Marmara University,* Istanbul, Türkiye

Abstract

Isolation and identification of protease and lipase producing moderately halophilic bacteria from soak liquor samples and studying their adverse effects to the sheepskin using scanning electron microscopy may provide critical data on decomposition of raw hide/skin materials during soaking process. Moreover, enzyme-production properties of the moderately halophilic isolates (such as catalase, oxidase, lipase, protease, urease, caseinase, amylase, cellulase, pullulanase, xylanase) were determined. The effects of different NaCl concentrations, pH and temperature values on the growth of moderately halophilic bacterial isolates were tested. In the present study, four moderately halophilic bacterial isolates were isolated and selected for further experiments. The isolated species designated as SLMHB5, SLMHB10, SLMHB12, SLMHB13 were similar to *Vibrio alginolyticus*, *Terribacillus halophilus*, *Vibrio alginolyticus*, and *Vibrio parahaemolyticus* species, respectively. Scanning electron micrographs of sheepskin samples demonstrated that enzymatic activities of moderately halophilic bacteria isolated from soak liquor samples which decomposed the skin structure. After 35-days storage period, the sheepskin sample showed bad odor, sticky appearance and hair slip. Hence, it is recommended to control these microorganisms during the soaking process with an effective antimicrobial agent.

Introduction

The leather industry is among the oldest traditional industries and it has a very important role in the world economy. The hides and skins, that are byproducts of the food industry, are processed and converted into valuable leather products in the leather industry. Fresh hides and skins are ideal growth environments for a wide variety of non-halophilic bacteria and yeasts originating from the animal itself and environmental sources.[1-3] If the fresh hides and skins are not preserved immediately, the enzymatic activities of these microorganisms may cause the deterioration of hides and skins. Traditionally, the hides and skins have been cured with salt or brine to remove water from the structure of hides and skins. However, the salt curing preservation process also causes contamination of hides and skins with moderately halophilic bacteria, halotolerant bacteria, extremely halophilic archaea, and haloversatile bacteria in the leather industry.[3-8] If the curing process is not accomplished adequately, metabolic activities of these microorganisms may cause bad odor, hair slip, and decomposition of hides and skins during storage and transportation periods which may decrease final leather quality.

The soaking process is the first stage in leather processing to remove preservation salt, non-collagenous proteins, and glycosaminoglycans. This process also cleans hides and skins from blood, manure, and dirt. In this process, salted hides and skins are rehydrated and collagen fibers return to the original hydrated structure by reabsorbing water.[9] Various researchers have found large numbers of microorganisms in soaked hides and soak liquors in the leather industry.[1,5,7,10-17] The microorganisms found on salted hide may grow in the soaking process.

Although moderately halophilic bacteria were reported on salted hides and skins, there are a limited number of studies related to moderately halophilic bacteria found in soak liquor.[18] In one of those papers, motile and aerobic moderately halophilic bacteria were isolated from drained soak liquor.[18] The researchers reported that total counts of moderately halophilic bacteria were detected as 2.3×10^5 CFU/mL-7.9×10^5 CFU/mL in the soak liquor samples.[18] In another preliminary study, total moderately halophilic bacterial counts, total proteolytic moderately halophilic bacteria, and total lipolytic moderately halophilic bacteria were investigated in twelve soak liquor samples collected from Tuzla Leather Organized Region (Tuzla, İstanbul/Türkiye).[19] The researchers reported that total moderately halophilic bacterial counts and proteolytic moderately halophilic counts were found as 1.8×10^4-4×10^6 CFU/mL and 1.2×10^4-1.4×10^6 CFU/mL, respectively. Lipolytic moderately halophilic bacterial counts were detected as 1×10^4-2×10^6 CFU/mL on Tween80 Agar Medium and 1×10^3-5.1×10^5 CFU/mL on Rhodamine B-Olive Oil Agar Medium, respectively.[19]

Vibrio alginolyticus, *Terribacillus halophilus*, and *Vibrio parahaemolyticus*, which are the test isolates in the present study, have also been isolated from different samples by other researchers. For instance, *Vibrio alginolyticus* was reported as a halophilic bacteria causing various diseases in marine animals such as fish,

*Corresponding author e-mail: pinar.caglayan@marmara.edu.tr
Manuscript received February 1, 2023, accepted for publication March 6, 2023.

crustaceans and molluscs.[20,21] Furthermore, *Vibrio alginolyticus* has been isolated from patients, brine shrimp, skin and sea water.[22-24] The species can cause enteric diseases in humans and animals.[25] It is among the important opportunistic bacterial pathogens.[26] *Vibrio alginolyticus* was reported as a naturally occurring organism in seafood, estuarine water and coastal waters[25] and a reservoir of virulence genes in aquatic environments.[27] It was also isolated from seawater samples,[28] the primary organism from moribund clam larvae,[20] diseased aquatic animals,[27] and saltpan soil samples.[29] The researchers stated that *Vibrio alginolyticus* isolates were able to produce lipase, caseinase, amylase, lecithinase and protease enzymes.[27,28] *Vibrio alginolyticus* isolates were able to grow at between pH 7.5-9, 10-40°C.[25]

Essghaier and colleagues used moderately halophilic *Terribacillus halophilus* isolate to improve the growth of tomatoes.[30] The intracellular antifungal enzyme (chitinase) produced by *Terribacillus halophilus* caused the reduction of spore germination of *Botrytis cinerea* and the treated tomato with moderately halophilic *Terribacillus halophilus* isolate could grow.[30] The intracellular enzymes of moderately halophilic bacteria can be used in biotechnological applications.[30,31] Pathogenic *Terribacillus halophilus* strains which are resistant to different disinfectants such as benzalkonium chloride, sodium hypochlorite and chloroxylenol were isolated from foods and surfaces of kitchen.[32] Some of these chemicals have been used in the food industry as well as in the leather industry. Microorganisms may develope resistance against chemicals due to the misuse of these and other antimicrobial agents. Endospore-forming *Terribacillus halophilus* has been isolated from soil and saltpan samples.[29,33] The investigators reported that *Terribacillus halophilus* showed growth at between pH 5-10, were motile and oxidase negative.[33] *Vibrio alginolyticus* and *Terribacillus halophilus* strains which were isolated from the saltpan soil samples collected from Vedaranyam were reported as protease and amylase producers.[29]

Vibrio parahaemolyticus was reported as a human pathogen found in marine environments.[34] *It is known as* an important seafood-borne pathogen causing vomiting, abdominal cramps, headache and diarrhea.[35] Urease-positive *Vibrio parahaemolyticus* was isolated from frozen sea foods, patients and sea water samples.[36] *Vibrio parahaemolyticus* was isolated from raw seafoods[34] and oyster samples.[37] *In another study, the Vibrio parahaemolyticus* strains isolated from oyster samples were shown to produce protease, lipase, caseinase and amylase.[37]

Due to the global economic importance of leather and related goods, determination of moderately halophilic bacteria in soak liquor is very important for leather industry to prevent their adverse effects. Consequently, in this study it was aimed to isolate and identify moderately halophilic bacteria from soak liquor samples. The effects of different NaCl concentrations, pH and temperature values on the growth of moderately halophilic bacterial isolates were tested. Enzyme-production properties of the isolates were also investigated. Moreover, the adverse effect of protease and lipase producing moderately halophilic bacteria on the sheepskin samples were also assessed using scanning electron microscope.

Experimental

Soak Liquor Samples

Four soak liquor samples were obtained from Tuzla Leather Organized Region (Tuzla, Istanbul/Türkiye) and placed into sterile bottles. The soak liquor samples were immediately brought to the laboratory on ice.

Isolation of Moderately Halophilic Bacteria from Soak Liquors

Twenty mL of soak liquor samples were put into glass bottle containing 180 mL of Sterile Physiological Saline Solution (SPSS) (10% sodium chloride) and the glass bottles were placed in an orbital shaker at 150 rpm for two hours at 24°C. 100 µL of direct and serial dilutions (10^{-1}-10^{-6}) of soak liquor solutions were spread onto the surface of the Complex Agar Medium (CAM) plates containing 5% yeast extract.[38,39] Finally, the salt concentration of test media was adjusted to 10% (w/v) with the following ingredients (SW10, saline water): 0.7% (w/v) $MgCl_2$, 8.1% (w/v) NaCl, 0.96% (w/v) $MgSO_4$, 0.2% (w/v) KCl, 0.036% (w/v) $CaCl_2$, 0.006% (w/v) $NaHCO_3$, and 0.0026% (w/v) NaBr.[38] The CAM plates were incubated at 37°C for 24 hours. After the incubation, different bacterial colonies were selected according to their colony properties. The selected bacterial colonies were streaked again to obtain pure isolates. The pure cultures were phenotypically and genotypically analyzed.

Molecular Characterization of Moderately Halophilic Isolates

The genomic DNA extraction was performed according to the QIAamp DNA MiniKit (Qiagen, Hilden/Germany). 16S rRNA gene was amplified with the universal primers 16F27-16R1488. The reactions of Polymerase Chain Reaction (PCR) amplification (95°C for 5 min, 25 cycles at 94°C for 1 min, 50°C for 1 min, 72°C for 2 min, final 10 min extension at 72°C) contained forward primer (2.5 µL), reverse primer (2.5 µL), PCR buffer (5 µL), dNTPs (10 mM, 8 µL), $MgCl_2$ (25 mM, 2.5 µL), *Taq* DNA Polymerase (0.5 µL), template DNA (1 µL), distilled water (28 µL), in a final volume of 50 µL.[40] The PCR products were purified using QIAquick PCR Purification Kit. The 16S rRNA gene sequence analysis were performed by Macrogen Inc. (Seoul, Korea). The comparison of 16S rRNA gene sequencing among the isolates and closely related species were determined further using ChromasPro (South Brisbane, Australia) and EzTaxon-e tool (Seoul, Korea).[41]

GenBank Accession Number

16S rRNA sequence data of the isolates SLMHB5, SLMHB10, SLMHB12, SLMHB13 reported in this paper, have been deposited in NCBI and GenBank nucleotide sequence database under the respective accession numbers: OP435723; OP435724; OP435725 and OP435727.

Cell Morphology and Pigmentation of Moderately Halophilic Isolates

The cell morphology and pigmentation of overnight cultures of each test isolate were investigated under optimal conditions. Gram staining was applied to each test isolate according to standard procedures.[42]

Effects of NaCl, pH and Temperature on Moderately Halophilic Bacterial Growth

Effect of different NaCl concentrations and optimum NaCl requirement of moderately halophilic bacteria were investigated on both CAM plates without salt and CAM plates containing different salt concentrations (0%, 1%, 2.5%, 5%, 7.5%, 10%, 12.5%, 15%, 17.5%, 20%, 22.5%, 25%, 27.5%, 30%). Effect of different pH values and optimum pH requirement were tested on CAM plates containing 10% NaCl at different pH values (4.0, 5.0, 6.0, 7.0, 8.0, 9.0, 10.0, 11.0, 12.0, 13.0). Moreover, the effect of different temperature values such as (4°C, 10°C, 20°C, 25°C, 30°C, 37°C, 40°C, 45°C, 50°C, 55°C, 60°C).[42]

Enzymatic Activities of Moderately Halophilic Isolates

Catalase activity

Catalase activity was tested by adding 3% H_2O_2 onto the bacterial colonies grown on CAM. The formation of bubbles on the bacterial colony was accepted as a positive catalase activity.[42]

Oxidase activity

Oxidase activity was investigated by spreading the colony of test isolate with a sterile loop onto the filter paper dropped with oxidase reagent. Immediate color change from pink to dark purple was accepted as positive oxidase activity.[42]

Lipase activity

Lipase activity was examined on the Tween80 Agar Medium (TW80M) containing Tween80 (1%, w/v). The inoculated agar plates were incubated for 48 hours at 37°C in an incubator. After incubation, the presence of opaque zones around the colonies on TW80M was taken as evidence of lipase activity.[43]

Protease activity

Protease activity was determined using Gelatine Agar Medium (GAM) containing gelatine (2%, w/v). The inoculated agar plates were incubated for 48 hours at 37°C in a incubator. After incubation, the plates containing GAM were flooded with Frazier solution. Clear zones around the colonies were accepted as an evidence of positive protease activity.[43]

Urease activity

Urease activity was examined on Christensen Urea Agar. After growth was obtained, the test tubes were checked for red or pink color.[44]

Caseinase activity

Caseinase production was tested on the Plate Count Agar medium containing 2% skim milk. After incubation, the clear zones around the bacterial colonies were accepted as positive activity of caseinase enzyme.[44]

Amylase activity

Amylase activity was tested on CAM prepared with 0.5% (w/v) starch. The incubated plates were flooded with iodine. Clear halos around the colonies accepted as positive amylase activity.[43]

Cellulase activity

Cellulase activity was tested on the cellulose agar medium prepared with 2 g carboxymethyl cellulose, 1 g casamino acid, 1 g yeast extract, 20 g agar and 1000 mL sterile saline water (10%).[44-46] The inoculated plates were incubated at 37°C for 24 hours.[44-46] After the incubation period, Congo Red (0.1%) solution was flooded on the bacterial colonies. Then, the plates were left for 30 minutes. After 30 minutes, the colonies on the plates were washed with 1 M NaCl solution. After the washing process, the clear zones around the bacterial colonies were accepted as positive cellulase activity.

Pullulanase and xylanase activities

Pullulanase and xylanase activities of the test isolates were examined on the plates containing the substrates azurine-cross-linked (AZCL)-pullulan and AZCL-xylan, respectively. Transparent zones observed around the colonies on xylan and pullulan media were accepted as positive xylanase and pullulanase activities.[43]

Curing Skins with Enzyme Producing Moderately Halophilic Isolates and Storage Period

The damage caused by the mixed culture of enzyme producing moderately halophilic bacterial isolates (*Vibrio alginolyticus*, *Terribacillus halophilus*, *Vibrio alginolyticus*, *Vibrio parahaemolyticus*) isolated from four soak liquor samples was investigated. Two pieces of freshly butchered sheep skin sample were obtained from the tannery. Thirty mL of brine solution (20% NaCl) and 10 g sheep skin pieces were mixed in two flasks. The sheep skin sample treated with only sterile brine solution was prepared as control. In sterile physiological saline solution (20% NaCl), each enzyme-producing isolates was suspended and this bacterial suspension adjusted to 0.5 McFarland turbidity standard (10^8 CFU/mL). Ten mL of each bacterial suspension was added

into the flask including brine solution and sheep skin sample. The flasks were shaken at 70 rpm at 24°C for 18 hours. Then, the cured sheep skin samples were taken from the flasks and stored at room temperature for 35 days. After the storage period, the samples were examined under the scanning electron microscope.[15] In addition, the organoleptic features (bad odor, sticky appearance, hair slip) were observed on the cured sheep skin samples during 35 days.

Preparation of Stored Skin Samples for Scanning Electron Microscope

Glutaraldehyde solution (4%) prepared with phosphate buffer (0.1 M, pH 7.2) was applied to sheep skin samples for 30 minutes. The sheep skin samples were washed three times for 10 min with the phosphate buffer (0.1 M). Osmium tetroxide (1%) prepared in phosphate buffer (0.1M) was applied to the sheep skins for one hour at 24°C. The samples were washed two times in sterile distilled water for 15 min and 95%, 75%, 50%, 35%, and absolute ethanol. The mixture of the ethanol-HMDS [1:2 (v/v)] (1×30 min), ethanol-hexamethyldisilazane (HMDS) [1:1 (v/v)] (1×30 min) and HMDS (2×30 min) were used during the air drying process. The sheepskin samples were put in a desiccator for 14 h. Then, the sheepskin samples were observed by Scanning Electron Microscope (Fei Quanta 450 FEG ESEM SEM, Model FEG 450).[47]

Results and Discussion

In the present study, three different moderately halophilic bacterial species -*Vibrio alginolyticus* (two isolates), *Vibrio parahaemolyticus* (one isolate), and *Terribacillus halophilus* (one isolate)- were isolated and identified from four soak liquor samples obtained from Tuzla Leather Organized Region (Tuzla, Istanbul/Türkiye) (Table I). All test isolates showed yellow pigmentation on the Complex Agar Medium. *Vibrio alginolyticus* and *Vibrio parahaemolyticus* were Gram-negative, *Terribacillus halophilus* was Gram-positive (Table

Table I

Phenotypic characteristics of the moderately halophilic bacterial isolates

Characteristics		*Vibrio alginolyticus*	*Terribacillus halophilus*	*Vibrio alginolyticus*	*Vibrio parahaemolyticus*
Isolate code		SLMHB5	SLMHB10	SLMHB12	SLMHB13
Pigmentation		yellow	yellow	yellow	yellow
Gram staining		-	+	-	-
Cell morphology		curved-rod	rod	curved-rod	curved-rod
NaCl range (%)		3-15	3-15	3-15	3-20
Optimum NaCl (%)		10	10	10	10
Temperature range (°C)		20-40	20-40	20-40	20-45
Optimum temperature (°C)		37	37	37	37
pH range		6-9	6-9	6-9	5-9
Optimum pH		7.0	7.0	7.0	7.0
Endospore formation		-	+	-	-
Motility		+	-	+	+
Production of indole		+	-	+	+
Citrate utilization		+	-	+	+
Hydrolytic Activities	Catalase	+	+	+	+
	Oxidase	+	-	+	+
	Lipase	+	+	+	+
	Protease	+	+	+	+
	Urease	+	+	+	+
	Caseinase	+	+	+	+
	Amylase	+	+	+	+
	Cellulase	-	-	-	-
	Pullulanase	-	-	-	-
	Xylanase	-	-	-	-

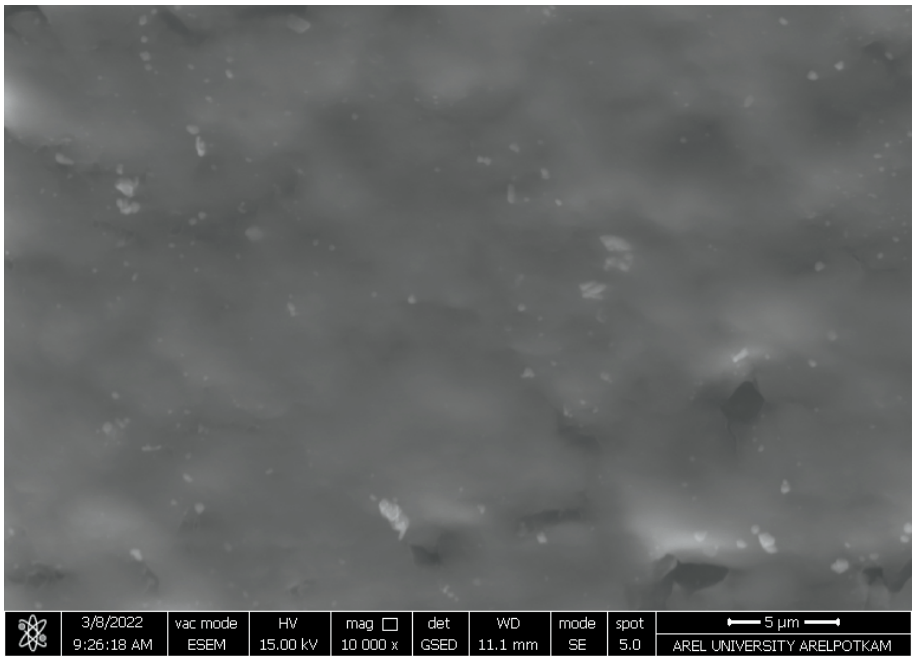

Figure 1. SEM micrographs of sheepskin sample treated with the sterile saline solution (control). The bar = 5 µm

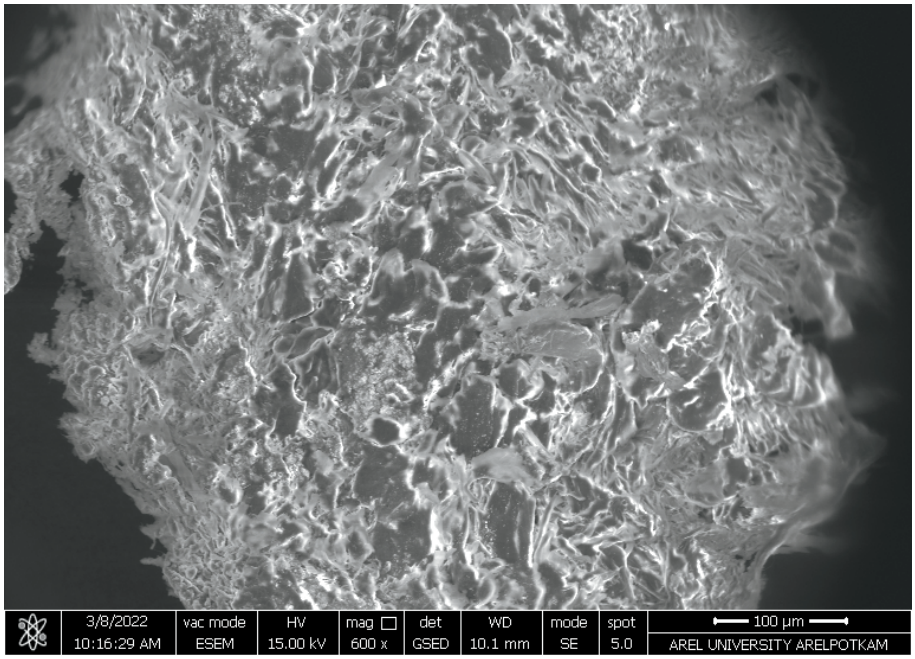

Figure 2. SEM micrographs of sheepskin sample treated with a mixed culture of moderately halophilic *Vibrio alginolyticus*, *Terribacillus halophilus*, and *Vibrio parahaemolyticus*. The bar = 100 µm

I). The cells of *Vibrio alginolyticus* and *Vibrio parahaemolyticus* were curved-rod, the cells of *Terribacillus halophilus* was rod-shaped. All isolates showed growth at 3-15% NaCl, 20-40°C and pH 6-9, *Vibrio parahaemolyticus* also showed growth at 20% NaCl, 45°C and pH 5. All test bacteria were able to grow at 10% NaCl, pH 7, 37°C (Table I). Hence, these isolates were considered as moderately halophilic. *Terribacillus halophilus* exhibited endospore formation. All isolates were motile, produced indole, and utilized citrate except *Terribacillus halophilus*. While all isolates produced catalase, lipase, protease, urease, caseinase, amylase, they did not produce cellulase, pullulanase and xylanase. Only *Terribacillus halophilus* was oxidase negative (Table I).

To examine adverse effect of lipase and protease producing moderately halophilic soak liquor isolates to the structure of sheepskin, sterile and freshly slaughtered sheep skin samples were cured with a mixed culture of test bacteria (*Vibrio alginolyticus*, *Terribacillus halophilus*, *Vibrio parahaemolyticus*) for 35 days at room temperature. As shown in Figure 1, the curing process of the sheepskins sample with the sterile saline solution protected the sheepskin structure against the

microbial damage during 35 days of storage period.

Figure 2 clearly demonstrates that the destructive effects of moderately halophilic bacterial cells of the mixed culture on the sheepskin structure. The mixed culture of the test isolate caused weakening fibers in the corium and splitting (Figure 2).

Changes in the organoleptic characterictics such as sticky appearance, hair slip, bad odor, and compactness of the sheepskin structure were also observed on the sheepskin sample treated with a mixed culture of moderately halophilic *Vibrio alginolyticus*, *Terribacillus halophilus*, and *Vibrio parahaemolyticus* (Figure 2). After the storage period, only the control sample (cured with sterile brine solution) did not show hair slip, bad odor and sticky appearance (Figure 1). In Figure 2, the compactness of collagen fibers of sheepskin sample was adversely affected by the enzymes produced by the test bacteria.

In a previous study, SEM micrographs showed that hides cured with protease producing extremely halophilic archaeal isolates caused red discoloration and grain damage after 49 days of storage time at 41°C.[15] In the study conducted by Birbir and her colleagues (2020), proteolytic and lipolytic extremely halophilic archaea (*Haloarcula salaria* AT1, *Halobacterium salinarum* 22T6, *Haloarcula tradensis* 7T3) were isolated from deteriorated salted sheepskin samples having red discolorations.[48] In that study, the freshly slaughtered sheepskin samples were cured with each test strain (*Haloarcula salaria* AT1, *Halobacterium salinarum* 22T6, *Haloarcula tradensis* 7T3), and with their mixed culture for 47 days at 33°C.[48] The researchers reported that organoleptic changes were closely related to enzymatic activities of the microorganisms.[48] They also reported that electron micrographs of each test isolate and their mixed culture destroyed the skins' collagen fibers.[48] In the present study, the structural damage of the sheepskin was due to the proteolytic and lipolytic activities of moderately halophilic bacteria,

Conclusion

This is the first study that investigates moderately halophilic bacterial species (*Vibrio alginolyticus*, *Terribacillus halophilus*, and *Vibrio parahaemolyticus*) found in the soak liquor samples obtained from Tuzla Leather Organized Region. All isolates produced catalase, lipase, protease, urease, caseinase and amylase enzymes. SEM micrographs of sheepskin sample treated with the mixed culture of moderately halophilic bacterial isolates also showed that these enzyme-producing isolates damaged the structure of the raw sheepskin sample. The experimental data obtained from this study clearly showed that inadequate preservation during soaking process may cause serious quality defects on crude sheepskins. Hence, effective antimicrobial applications should be applied in the soaking process to obain high quality leather product in the leather industry.

References

1. Birbir, M., Ilgaz, A.; Isolation and Identification of Bacteria Adversely Affecting Hide and Leather Quality. *J. Soc. Leather Technol.Chem.* **80**, 147-153, 1996.
2. Oppong, D., Bryant, S., Rangarajan, R., Steele, S., Radwell, D., Hyllengren, L.; Application of Molecular Techniques to Identify Bacteria Isolated From the Leather Industry. *JALCA* **101**, 140-145, 2006.
3. Ulusoy, K., Birbir, M.; Identification and Metabolic Activities of Bacterial Species Belonging to the *Enterobacteriaceae* on Salted Cattle Hides And Sheep Skins. *JALCA* **110**, 86-199, 2015.
4. Kallenberger, W.E.; Halophilic Bacteria in Hide Curing, *PhD Thesis*, Division of Graduate Studies and Research of the University of Cincinati, Department of Basic Science Tanning Research of the Collage of Arts and Science, 1985.
5. Bailey, D.G., Birbir, M.; A Study of the Extremely Halophilic Microorganisms Found on Commercially Brine-Cured Cattle Hides. *JALCA* **88**, 285-293, 1993.
6. Birbir, M.; Tuzla Muhafaza Edilmiş Fransız ve Rus Derilerinin Halofilik Bakteriler Yönünden İncelenmesi. *Journal of Turkish Microbiology Society* **27**, 68-73, 1997.
7. Berber, D., Birbir, M.; Examination of Bacterial Populations in Salt, Salted Hides, Soaked Hides and Soak Liquors. *JALCA* **105**(10), 320-326, 2010.
8. Caglayan, P.; Enzymatic Reactions and Phylogenetic Analysis of Haloversatile Bacteria Isolated from Çamaltı Saltern Salt Samples used in Leather Industry. *JALCA* **115**, 450-461, 2019.
9. Buljan, J., Kral, I.; The Framework for Sustainable Leather Manufacture, United Nations Industrial Development Organization (UNIDO), 1-212, 2015.
10. Aslan, E., Birbir, M.; Examination of Gram-positive Bacteria on Salt-pack Cured Hides. *JALCA* **106** (12), 372-380, 2011.
11. Aslan, E.; Birbir, M.; Examination of Gram-negative Bacteria on Salt-pack Cured Hides. *JALCA* **4**(107), 106-115, 2012.
12. Berber, D., Birbir, M.; Determination of Major Problems of Raw Hide and Soaking Process in Leather Industry. *Int. J. Adv. Eng. Pure Sci.* **2**, 118-125, 2019.
13. Berber, D., Birbir, M., Mertoglu, B.; Examination of Archaeal and Bacterial Populations in Salt, Salted and Soaked Hide and Soak Liquor Samples via Fluorescent in Situ Hybridization. *J. Soc. Leather Technol.Chem.* **94**(6), 259-261, 2010.
14. Berber, D., Birbir, M., Hacioglu, H.; Efficacy Assessment of Bactericide Containing Didecyldimethylammonium Chloride on Bacteria Found in Soak Liquor at Different Exposure Times. *JALCA* **105**(11), 354-359, 2010.
15. Bailey, D.G., Birbir, M.; The Impact of Halophilic Organisms on the Grain Quality of Brine Cured Hides. *JALCA* **91**(2), 1996.
16. Bailey, D.G.; The Preservation of Hides and Skins. *JALCA* **98**, 308-319, 2003.

17. Birbir, M., Kallenberger, W., Ilgaz, A., Bailey, G.; Halophilic Bacteria Isolated from Brine Cured Cattle Hides. *J. Soc. Leather Technol.Chem.* **80**, 87-90, 1996.
18. Gosh, R., Chattopadhyay, P., Chattopadhyay, B.; Antibiotic Resistance Profile of Halophilic Microorganisms Isolated from Tannery Effluent. *Indian J. Biotechnol.* **9**(1), 80-86, 2010.
19. Birbir, M., Caglayan, P.; Moderately Halophilic Bacteria in Soak Liquors in Leather Industry. AMB2022, I. International Advances in Molecular Biology Congress, September 19-22, 2022.
20. Gómez-León, J., Villamil, L., Lemos, M.L., Novoa, B., Figueras, A.; Isolation of *Vibrio alginolyticus* and *Vibrio splendidus* from Aquacultured Carpet Shell Clam (*Ruditapes decussatus*) Larvae Associated with Mass Mortalities. *Appl. Environ. Microbiol.* **71**(1), 98-104, 2005.
21. Kahla-Nakbi, A.B., Besbes, A., Chaieb, K., Rouabhia, M., Bakhrouf, A.; Survival of *Vibrio alginolyticus* in Seawater and Retention of Virulence of its Starved Cells. *Mar. Environ. Res.* **64**(4), 469-478, 2007.
22. Smolikova L.M., Lomov L.M., Khomenko T.V., Murnachev G.P., Kudriakova T.A., Fetsailova O.P., Sanamiants E.M., Makedonova L.D., Kachkina G.V., Golenishcheva E.N.; Studies on Halophilic Vibrios Causing a Food Poisoning Outbreak in the City of Vladivostok. Zh. *Mikrobiol. Epidemiol. Immunobiol.* **6**, 3-7, 2001.
23. Xie, Z.Y., Hu, C.Q., Chen, C., Zhang, L.P., Ren, C.H.; Investigation of Seven *Vibrio* Virulence Genes Among *Vibrio alginolyticus* and *Vibrio parahaemolyticus* Strains from the Coastal Mariculture Systems in Guangdong, China. *Lett. Appl. Microbiol.* **41**, 202-207, 2005.
24. Scheftel, J.M., Ashkar, K., Boeri, C., Monteil, H.; Phlegmon au doigt à *Vibrio alginolyticus* consécutif à une blessure chez un patient de retour du Maroc. *Journées Francophones de Microbiologie des Milieux Hydriques*, 23-24 November 2006.
25. Mustapha, S., Mustapha, E.M., Nozha, C.; *Vibrio Alginolyticus*: An Emerging Pathogen of Foodborne Diseases. *Int. J. Sci. Technol.* **2**(4), 302-309, 2013.
26. George, M., John, K., Iyappan, T., Jeyaseelan, M.; Genetic Heterogeneity Among *Vibrio alginolyticus* Isolated from Shrimp Farms by PCR Fingerprinting. *Lett. Appl. Microbiol.* **40**, 369-372, 2005.
27. Bunpa, S., Sermwittayawong, N., Vuddhakul, V.; Extracellular Enzymes Produced by *Vibrio alginolyticus* Isolated from Environments and Diseased Aquatic Animals. *Procedia Chemistry* **18**, 12-17, 2016.
28. Hörmansdorfer, S., Wentges, H., Neugebaur-Büchler, K., Bauer, J.; Isolation of *Vibrio alginolyticus* from Seawater Aquaria. *Int. J. Hyg. Environ. Health* **203**(2), 169-175, 2000.
29. Manikandan, P., Gnanasekaran, A., Senthilkumar, P.K; Screening and Characterization of Protease Producing Halophilic Bacteria from Saltpan Area Vedaranyam, Tamil Nadu. *Int. J. Pharm. Biol. Sci.* **8**(4), 160-168, 2018.
30. Essghaier, B., Dhieb, C., Rebib, H., Ayari, S., Abdellatif Boudabous, A.R., Sadfi-Zouaoui, N.; Antimicrobial Behavior of Intracellular Proteins from Two Moderately Halophilic Bacteria: Strain J31 of *Terribacillus halophilus* and Strain M323 of *Virgibacillus marismortui*. *J. Plant Pathol. Microb.* **5**(1), 1-7, 2014.
31. Caglayan, P., Birbir, M., Sánchez-Porro, C., Ventosa, A.; Detection of Industrially Potential Enzymes of Moderately Halophilic Bacteria on Salted Goat Skins. *Turk. J. Biochem.* **43**, 312-322, 2018.
32. Al-Johny, B.O., Alkhuzaee, A.M.; Isolation and Identification of Pathogenic Bacteria Showing Resistance against Disinfectants. *J. Pure Appl. Microbiol.* **13**(4), 2065, 2019.
33. An, S.Y., Asahara, M., Goto, K., Kasai, H., Yokota, A.; *Terribacillus saccharophilus* gen. nov., sp. nov. and *Terribacillus halophilus* sp. nov., Spore-forming Bacteria Isolated from Field Soil in Japan. *Int. J. Syst. Evol. Microbiol.* **57**, 51-55, 2007.
34. Su, Y.C., Liu, C.; *Vibrio parahaemolyticus*: A Concern of Seafood Safety. *Food Microbiol.* **24**(6), 549-558, 2007.
35. Kaysner, C.A., DePaola, A.; *Vibrio*. In: Downes, F.P., Ito, K. (Eds.), Compendium of Methods for the Microbiological Examination of Foods, fourth ed. American Public Health Association, Washington, DC, pp. 405-420, 2001.
36. Honda, S., Matsumoto, S., Miwatani, T., Honda, T.; A Survey of Urease-positive *Vibrio parahaemolyticus* Strains Isolated from Traveller's Diarrhea, Sea Water and Imported Frozen Sea Foods. *Eur. J. Epidemiol.* **8**(6), 861-864, 1992.
37. Costa, R.A., Conde Amorim, L.M., Araújo, R.L., Fernandes Vieira, R.H.S.; Multiple Enzymatic Profiles of *Vibrio parahaemolyticus* Strains Isolated from Oysters. *Revista Argentina de Microbiología* **45**(4), 267-270, 2013.
38. Ventosa, A., García, M.T., Kamekura, M., Onishi, H., Ruíz-Berraquero, F.; *Bacillus halophilus* sp. nov., a Moderately Halophilic *Bacillus* Species. *Syst. Appl. Microbiol.* **12**, 162-166, 1989.
39. Caglayan, P., Birbir, M., Ventosa, A., Sánchez-Porro, C.; Characterization of Moderately Halophilic Bacteria from the Salt-pack Cured Hides. *J. Soc. Leather Technol.Chem.* **99**(5), 250-254, 2015.
40. Mellado, E., Nieto, J.J., Ventosa, A.; Phylogenetic Interferences and Taxonomic Consequences of 16S Ribosomal DNA Sequence Comparison of *Chromohalobacter marismortui*, *Volcaniella eurihalina* and *Deleya halophila* and Reclassification of *V.eurihalina* as *Halomonas eurihalina* comb. nov. *Int. J. Syst. Bacteriol.* **45**, 712-716, 1995.
41. Kim, O.S., Cho, Y.J., Lee, K., Yoon, S.H., Kim, M., Na, H., Park, S.C., Jeon, Y.S., Lee, J.H., Yi, H., Won, S., Chun, J.; Introducing EzTaxon: a Prokaryotic 16S rRNA Gene Sequence Database with Phylotypes that Represent Uncultured Species. *Int. J. Syst. Evol. Microbiol.* **62**, 716-721, 2012.
42. Sánchez-Porro, C., Yilmaz, P., De La Haba, R.R., Birbir, M., Ventosa, A.; *Thalassobacillus pellis* sp. nov., a Moderately Halophilic, Gram-positive Bacterium isolated from Salted Hides. *Int. J. Syst. Evol. Microbiol.* **5**, 1206-1210, 2011.
43. Sánchez-Porro, C., Martin, S., Mellado, E., Ventosa, A.; Diversity of Moderately Halophilic Bacteria Producing Extracellular Hydrolytic Enzymes. *J. Appl. Microbiol.* **94**, 295-300, 2003.

44. Caglayan, P., Birbir, M., Sánchez-Porro, C., Ventosa, A.; Screening of Industrially Important Enzymes Produced by Moderately Halophilic Bacteria Isolated from Salted Sheep Skins of Diverse Origin. *JALCA* **112**(06), 207-216, 2017
45. Limauro, D., Cannio, R., Fiorentino, G., Rossi, M., Bartolucci, S.; Identification and Molecular Characterization of an Endoglucanase Gene, celS, from the Extremely Thermophilic Archaeon *Sulfolobus solfaraticus*. *Extremophiles* **5**, 213-219, 2001.
46. Birbir, M., Calli, B., Mertoglu, B., Bardavid, R.E., Oren, A., Ogmen, M. N., Ogan, A.; Extremely Halophilic Archaea from Tuz Lake, Turkey, and The Adjacent Kaldirim and Kayacik salterns. *World J. Microbiol. Biotechnol.* **23**, 309-316, 2007.
47. Das Murtey, M., Ramasamy, P.; Sample Preparations for Scanning Electron Microscopy-Life Sciences, Intech, Chapter 8, 161-185, 2016.
48. Birbir, M., Caglayan, P., Birbir, Y.; The Destructive Effects of Extremely Halophilic Archaeal Strains on Sheepskins, and Proposals for Remedial Curing Processes Use of Sterile Brine or Direct Electric Current to Prevent Red Heat Damage on Salted Sheepskins. *Johnson Matthey Technol. Rev.* 64(4), 489-503, 2020.

Tanning with Pomegranate Peel Tannin

by
Cigdem Kilicarislan Ozkan
Faculty of Engineering, Department of Leather Engineering, Ege University, 35100 Bornova, Izmir, Turkey

Abstract

By-products of pomegranate juice enterprises are evaluated as a "green" raw material for many industries. In this study, pomegranate peels which are well known with high polyphenolic content were evaluated as a potential source of tanning agent for leather industry. For this purpose, firstly pomegranate peels were extracted in Koch extractor at 70°C for 8 hours. In order to determine the tanning ability, 30% of ground pomegranate peel powder (containing 7.2% of active tannin matter) was used in the tanning process and pomegranate peel tanned leather was evaluated in terms of increases in thickness and shrinkage temperature, color change and mechanical properties. The application of pomegranate peel tannin in the tanning process provided that an acceptable shrinkage temperature (68.5°C) and mechanical properties for vegetable tanned leathers. The results revealed that the tannin obtained from pomegranate peel has a remarkable tanning effect and can be used in the tanning process. Thus, it is concluded that pomegranate peels can be evaluated as a new source of tannin for leather industry.

Introduction

Polyphenol-rich plant extracts (vegetable tannins) bearing a large number of hydroxyl and other functional groups have ability to form strong linkages with collagen.[1] Therefore, vegetable tannins are taken into consideration as eco-friendly and manageable tanning agents and they contribute to remarkable improvement in leather properties by tanning process.[2] Vegetable tanning technology was prevalent process for leather industry over centuries until it has gradually been displaced to chrome tanning by the end of the 19th century.[1] However, vegetable tanning agents have recently regained their former popularity due to the increasing interest and even compelling trend towards more sustainable, greener and eco-friendly tanning processes. On the other hand, the vegetable tannin sources having commercial importance for tanning are limited due to scarce number of tannin rich plant materials. In recent years, numerous researchers have been focused on searching for new tannin sources that can be used in leather industry as tanning agent.[3-6]

Among the alternative tannin sources, pomegranate peels which are generated as waste in fruit juice enterprises have recently attracted the attention of many industries.[7-10] The peels constitute 30-40% of the pomegranate fruit and they remain as a byproduct after juicing fruit. On a global scale, there are 3 million tons of total pomegranate production, resulting in approximately 1.62 million tons of waste.[11] Due to their high polyphenolic content and antioxidant properties, pomegranate peels are no longer considered as waste, but as a valuable raw material source for sustainable, eco-friendly and green chemical production.

From the literature review, it was seen that there is limited data available concerning the possible usability of pomegranate peels as a source of tanning agent and its detailed tanning properties.[2,12] So, as the first step pomegranate peel tannin was decided to be used as a retanning agent in leather processing and besides its retanning performance, its effect on prevention of Cr(VI) formation was investigated in a previous study.[13] Especially the high tannin content and considerable filling properties obtained from the study drove to investigate its solo performance. Thus, as a complementary study, in the present part, it was focused on investigation of pomegranate peel tannin's tanning performance as a main tanning agent.

Materials and Methods

Materials

The pomegranate peels were supplied from a food company operating in Torbali/Izmir. Before experiments, pomegranate peels were rinsed, dried and broken into pieces similarly the previous study.[13] Pickled sheep skins (breed of Métis) were used in tanning trials.

Methods

Tannin extraction: Extraction of pomegranate peels was carried out in a similar way as described in the previous study.[13] From the evaluation of the findings obtained from the previous study, it was seen that higher extraction temperature did not have a significant contribution to the extraction yield and tannin content, so the extractions were carried out at 70°C in the present study.

Re-determination of the tannin content by repeating extraction processes has required due to following reasons: a) It should not be ignored that the tannin content of pomegranate peels may change more or less on account of different harvest times. The presence

Corresponding author email: cigdem.kilicarislan@ege.edu.tr
Manuscript received February 1, 2023, accepted for publication March 10, 2023.

of tannin can differ from plant to plant, and part to part of a plant since plant polyphenolic compounds are produced naturally. b) In order to accurately calculate the amount of tannin to be used in tanning process, the tannin content of the raw material to be used must be known exactly. Extraction yield was calculated according to Formula 1.

$$(\%)\ \text{Extraction Yield} = (\text{extract obtained (g)}/\text{pomegranate peels used (g)}) \times 100 \quad (1)$$

Tannin and non-tannin matter contents of obtained extract were determined according to the SLC 114.[14] 115,[15] 116[16] and 117[17] test methods. All analyses were repeated three times and mean data were given.

Tanning with Pomegranate Peel: Pomegranate peels were ground by micro mill (Super Mixer SM 108) into powder form before the tanning process. Approximately 30% of ground pomegranate peel powder (containing 7.2% of active tannin matter considering the determined tannin content) was weighed by taking in account the weight of intact pelt and used in tanning process in order to determine tanning effect. The applied tanning recipe is given in Table I. It should be pointed out that the recipe was not prepared to manufacture of garment, shoe upper etc., only a basic tanning recipe was applied to determine the tanning effect of pomegranate peels.

Determination of tanning properties of pomegranate peel: Filling coefficient and shrinkage temperature, the most important indicators

Table I

Tanning recipe

Process	Amount (%)	Product	Temperature (°C)	Duration (min.)	pH
Depickling	150	Water (8 °Be´ NaCl)	28-30	15	
	1	HCOONa		40	
	0.3	$NaHCO_3$		60	4.8
Draining - Thickness Measurement					
Tanning	70	Water	35		
	10	Ground Pomegranate Peel		90	
	10	Ground Pomegranate Peel		90	
	10	Ground Pomegranate Peel	37	90 (left in bath overnight 7-8 rpm)	
	0.1	Fungicide		20	
	0.7	HCOOH		60	3.7
Washing	200	Water		10	
Draining - Thickness Measurement Aging for 1 week - Shrinkage Temperature Measurement					
Retanning-Fatliquoring	200	Water	35		
	1	Neutralizing Syntan		30	5.0
	3	Amphoteric Acrylic Polymer		30	
	4	Sulphited Natural Fatliquor	45	75	
	3	Synthetic Fatliquor			
	3	Lanolin Fatliquor			
	0.8	HCOOH		90	3.6
Washing	200	Water		10	

for qualifying tanning effect, of tanned leather were determine in order to evaluate tanning properties of pomegranate peel. Before tanning (after depickling process) the thicknesses of pelt (T_1) and after tanning the thickness of leather (T_2) were measured from 8 different points in wet form according to ISO 2589[18] and mean data were determined. Filling coefficient was calculated according to Formula 2.

$$(\%)\ \text{Filling coefficient} = ((T_2 - T_1) / T_1) \times 100 \qquad (2)$$

The shrinkage temperatures of intact pelt and tanned leather were determined according to ISO 3380[19] with three repetitions and mean data was given.

Measurement of color: The color and color components of pomegranate peel tanned leather were measured by using the Minolta CM-2600d Spherical Spectrophotometer according to the CIE*Lab color system. Color measurements were taken from 15 different parts of the leather sample and the result was given as mean value.

Physical Properties of Tanned Leather: In order to determine the mechanical properties of pomegranate peel tanned leather, the tensile strength and percentage of elongation[20] and tear load[21] of the leather were determined. Samples for the tests were taken in accordance with ISO 2418[22] standard. The samples were conditioned according to the ISO 2419[23] standard and their thicknesses were measured according to the ISO 2589[18] standard. For both tests, 3 parallel and 3 perpendicular samples were taken, and the test results were given as the mean value.

Results and Discussion

Extraction Yield and Tannin Content of Pomegranate Peel: During the extraction of plant materials, water-soluble/insoluble non-tannin matters (such as sugars, salts, flavones, gallic acid, other acids, etc.) also pass into the extract as well as tannins. Looking from the viewpoint of the tanning process, although non-tannin matters do not have tanning properties, their presence in the tanning bath may affect the character of produced leather. The tannin/non-tannin and soluble/insoluble matter contents of pomegranate peel extract are given in Figure 1. The extraction yield was determined to be 44.5(±0.2)%.

Gurler[12] reported that the pomegranate peels, which were supplied from a company as a ready extract, contain 37.2% tannin and 72.1% total soluble matter and El Maujahed et al.[2] reported that 38.2% of extraction yield was obtained from the extraction of pomegranate peels with distilled water in 1:10 ratio for 12 hours at 100°C in the dark ambient by use of ethanol as an additive.

According to the results, it was seen that the extraction yields and tannin contents differ in pomegranate peels. Many factors such as harvest time, supplied region and extraction conditions can be effective for this variation.

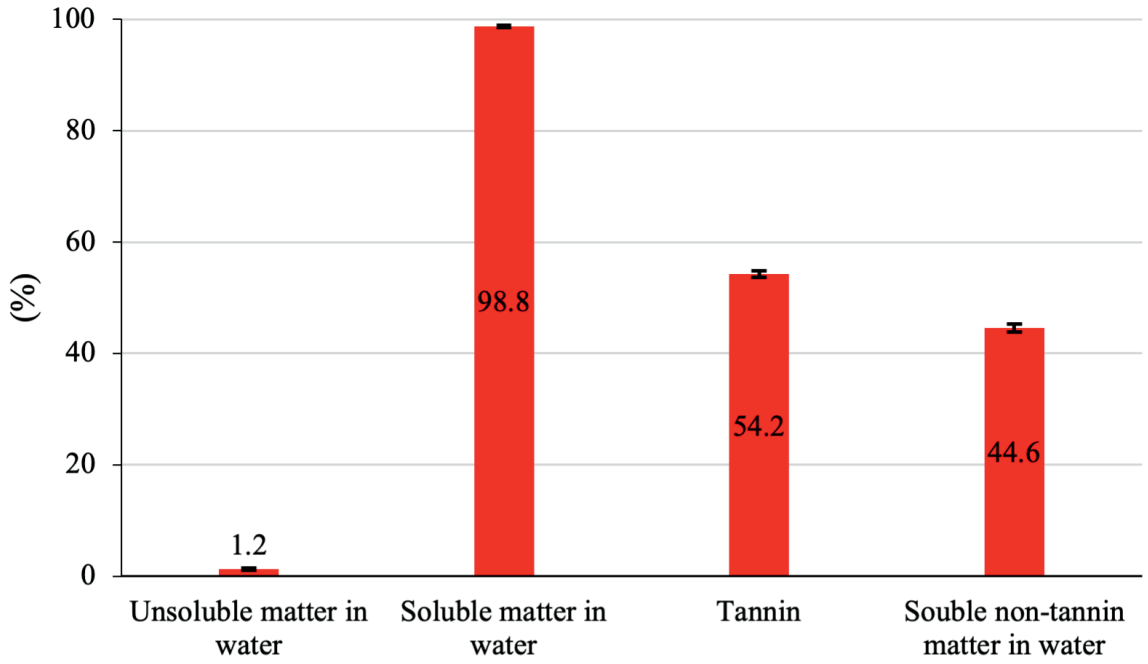

Figure 1. Tannin/non-tannin and soluble/non-soluble matter contents of pomegranate peel extract.

Table II

Comparison of commercially available tannins and tannin sources

Tannin	Tannin Type	Part of Plant	% Tannin in extract	% Tannin content in plant part
Mimosa	Condensed	Bark	70	36
Qubracho	Condensed	Wood	70	21
Chestnut	Hydrolysable	Wood	75	10
Olive	Hydrolysable	Leaf	28	10
Pomegranate	Hydrolysable	Peel	54	24
Sumach	Hydrolysable	Leaf	50	20
Tara	Hydrolysable	Pods	50	40
Gambier	Condensed	Leaf	50	25

In Table II, a comparison of commercially available tannins and tannin sources are given above (since there are various types of plants and different plant species having various amounts of tannin contents even for a type of tannin, in this table are approximate values).

Tanning properties of pomegranate peel: The shrinkage temperatures and thicknesses of intact pelt and the leather treated with pomegranate peels are given in Table III. From the results, it was clearly seen that tanning with pomegranate peels resulted in a remarkable increase in shrinkage temperature (26.8°C) and filling coefficient (57.1%) comparing with the intact pelt. From the evaluation of the shrinkage temperature and filling coefficient results, it was deduced that pomegranate peel tannin has an effective tanning ability.

Pomegranate peel extract solutions at different ratios (15, 20, 30%) were used in tanning process of garment leathers by Gurler[12] and it was stated that the highest shrinkage temperature was obtained to be 79°C with 15% of pomegranate peel. However, controversially, it was also specified that as the amount of used pomegranate peel extract increased, the shrinkage temperature decreased to 74°C.

Color of tanned leather: Leathers tanned with vegetable tannins possess the characteristic color of the tannins used. This type of leather is either not dyed through or dyed in pastel or dark tones, arbitrarily. For this reason, it is important to determine the final color of leather tanned with pomegranate peel. Table IV shows the L, a, b values obtained from color measurements of the tanned leather. From the examination of the data, it was seen that the color of the leather tanned with pomegranate peel is predominantly in yellow tones and contains a slight reddish tone.

Mechanical properties of tanned leather: Physical test results of leather tanned with pomegranate peel are given in Table V. It can be obviously seen that the obtained tensile (20.1 N/mm^2) and

Table III

Thickness and shrinkage temperature values of intact pelt and tanned leather

	Thickness (mm)	Shrinkage temperature (°C)
Intact pelt	0.7(±0.5)	41.7(±0.6)
Tanned leather	1.1(±0.4)	68.5(±0.7)

Table IV

Color measurement values of leather tanned with pomegranate peel

L	a	b
75.7(±0.6)	3.2(±0.3)	28.3(±0.7)

Lightness/brightness (L=0 black, L=100 white),
red/green color (+a red, -a green) and yellow/blue color (+b yellow, -b blue).

Table V

Mechanical properties of leather tanned with pomegranate peel

Tensile Strength (N/mm^2)	Elongation at break (%)	Tear Strength	
		Max. Force (N)	Thickness (mm)
20.1(±2.9)	71.2(±5.4)	32.0(±1.5)	0.7(±0.02)

tear (45.7 N/mm) strengths met the acceptable quality standards recommended by United Nations Industrial Development Organization (UNIDO)[24] for vegetable tanned upholstery leathers (<2 mm of thickness, 10 N/mm^2 for tensile strength and 15 N/mm for tear strength). In addition, the obtained values also met the quality requirements for garments leathers recommended by UNIDO[24] regardless of the tanning method (min. tensile strength of 12 N/mm^2 and min. tear strength of 20 N/mm).

In literature, related to the mechanical properties of the leathers tanned with pomegranate peel; Gurler[12] reported that the highest tensile and tear strength values of pomegranate peels tanned leathers were found to be 6.3 N/mm^2 and 17.4 N/mm, respectively.

Conclusion

In this study, the tanning ability of pomegranate peel tannin and its possible utilization as a main tanning agent in leather industry were investigated. For this purpose, after determining the tannin content of the pomegranate peels, a basic tanning process was applied using 30% of ground pomegranate peel powder (containing 7.2% active tannin matter considering the determined tannin content). Considering the filling coefficient (which is also a sign of fiber isolation), shrinkage temperature and physical properties of the tanned leather, it was concluded that pomegranate peels (containing remarkable polyphenolic compounds) which arise from as a waste in fruit juice enterprises can be utilized as a new source of vegetable tanning agent.

In case of using ground pomegranate peel powder instead of extraction product, it is crucial to determine the tannin content of pomegranate peels, since the tannin content of pomegranate peels may change more or less on account of different harvest times, in order to accurately calculate required amount of tannin to be used in tanning process according to different types of vegetable tanned leather articles.

However, it is necessary to emphasize here that tanning with increasing amounts of pomegranate peel powder bearing higher amounts of active tanning matters i.e. 11-15% (which is generally required for different types of vegetable tanned leather articles) will result in much better tanning performance and leather characteristics.

References

1. Valeika, V., Sapijanskaite, B., Sirvaityte, J., Plavan, V., Alaburdaite, R.; Potentilla Erecta (L.) Raeusch as an alternative source of environmentally friendly polyphenols for Leather Tanning. *JALCA* **113**, 183-191, 2018.
2. El Moujahed, S., Errachidi, F., Abou Oualid, H., Botezatu-Dediu, A.V., Chahdi, F.O., Rodi, Y.K., Dinica, R.M.; Extraction of insoluble fibrous collagen for characterization and crosslinking with phenolic compounds from pomegranate byproducts for leather tanning applications. *RSC Adv* **12**, 4175-4186, 2022. https://doi.org/10.1039/D1RA08059H
3. Conde, M., Combalia, F., Olle, L., Bacardit, A.; Pine tannin extraction from residues of pine forest exploitation. *JALCA* **115 (6)**, 215-221, 2020.
4. China, C.R., Nyandoro, S.S., Munissi, J.J.E., Maguta, M.M., Meyer, M., Schroepfer, M.; Tanning capacity of *Tessmannia burttii*extracts: the potential eco-friendly tanning agents for the leather industry. *J Leather Sci Eng* **3(13)**, 1-9, 2021. https://doi.org/10.1186/s42825-021-00055-2
5. Das, R.K., Mizan, A., Zohra, F.T., Ahmed, S., Ahmed, K.S., Hossain, H.; Extraction of a novel tanning agent from indigenous plant bark and its applicationin leather processing. *J Leather Sci Eng* **4(18)**, 1-15, 2022. https://doi.org/10.1186/s42825-022-00092-5
6. Nasr, A.I., Shaer, E., Elraheem, A.; Evaluation of potential application for guava bark extract in leather tanning. *Egypt J Chem* **65(11)**, 199-208, 2022. https://doi.org/10.21608/ejchem.2022.118540.5335
7. Negi, P.S., Jayaprakasha, G.K., Jena, B.S.; Antioxidant and antimutagenic activities of pomegranate peel extracts. *Food Chem* **80(3)**, 393–397, 2003. https://doi.org/10.1016/S0308-8146(02)00279-0
8. Singh, B., Singh, J.P., Kaur, A., Singh, N.; Phenolic compounds as beneficial phytochemicals in pomegranate (Punica granatum L.) peel: A review. *Food Chem* **261**, 75–86, 2018. https://doi.org/10.1016/j.foodchem.2018.04.039
9. Ajmal, M., Adeel, S., Azeem, M., Zuber, M., Akhtar, N., Iqbal, N.; Modulation of pomegranate peel colourant characteristics for textile dyeing using high energy radiations. *Ind Crops Prod* **58**, 188-193, 2014. https://doi.org/10.1016/j.indcrop.2014.04.026
10. Saad, H., Charrier-El Bouhtoury, F., Pizzi, A., Rode, K., Charrier B., Ayed, N.; Characterization of pomegranate peels tannin extractives. *Ind Crops Prod* **40**, 239–246, 2012. https://doi.org/10.1016/j.indcrop.2012.02.038
11. Magangana, T.P., Makunga, N.P., Fawole, O.A., Opara, U.L.; Processing Factors Affecting the Phytochemical and Nutritional Properties of Pomegranate (Punica granatum L.) Peel Waste: A Review. *Molecules* **25**, 4690, 2020. https://doi.org/10.3390/molecules25204690
12. Gurler, D.K; Tannin content of pomegranate rind extract and its potential use in leather production. *Fresenius Environ Bull* **25(12A)**, 5924-5928, 2016.

13. Kilicarislan Ozkan, C.; Valorization of pomegranate peel waste as retanning agent in leather industry and investigation of its effect on prevention of Cr(VI) formation. *JALCA,* **118**, 51-58, 2023.
14. SLC 114, Determination of Total Solids, Society of Leather Technologists and Chemists Official Methods of Analysis, 1996.
15. SLC 115, Determination of Total Solubles, Society of Leather Technologists and Chemists Official Methods of Analysis, 1996.
16. SLC 116, Determination of Non-tannin Constituents, Society of Leather Technologists and Chemists Official Methods of Analysis, 1996.
17. SLC 117, Determination of Tannin Matter Absorbable by Hide Powder, Society of Leather Technologists and Chemists Official Methods of Analysis, 1996.
18. ISO 2589 [IULTCS/IUP 4], Leather - Physical and mechanical tests - Determination of thickness, 2016.
19. ISO 3380 [IULTCS/IUP 16], Leather - Physical and mechanical tests - Determination of shrinkage temperature up to 100 °C, 2015.
20. ISO 3376 [IULTCS/IUP 6], Leather - Physical and mechanical tests - Determination of tensile strength and percentage elongation, 2020.
21. ISO 3377-2 [IULTCS/IUP 8], Leather - Physical and mechanical tests - Determination of tear load-Part 2: Double edge tear, 2016.
22. ISO 2418 [IULTCS/IUP 2], Leather - Chemical, physical and mechanical and fastness tests - Sampling location, 2017.
23. ISO 2419 [IULTCS/IUP 1, IULTCS/IUP 3], Leather - Physical and mechanical tests - Sample preparation and conditioning, 2012.
24. United Nations Industrial Development Organization (UNIDO), Acceptable quality standards in the leather and footwear industry, 1994. https://leatherpanel.org/sites/default/files/publications-attachments/acceptable_quality_standards_in_the_leather_and_footwear_industry.pdf (accessed 06 December 2022)

LEATHER

AVELLISYNCO

Selected Dyestuffs

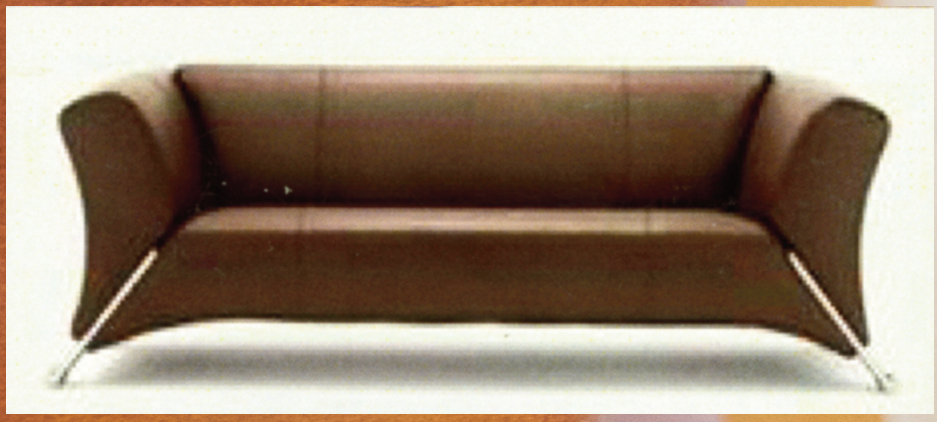

CHEMTAN

17 Noble Farm Drive • Lee, NH 03861 (Office)
57 Hampton Road • Exeter, NH 03833 (Manufacturing)
Tel: (603) 772-3741 • Fax: (603) 772-0796
www.CHEMTAN.com

Industry News

Professor Jianzhong Ma Announced as Recipient of the IULTCS Merit Award 2023

It is with great pleasure that IULTCS announces Prof Jianzhong Ma has been chosen as the winner of the prestigious IULTCS Merit Award for Excellence in the Leather Industry. The IULTCS was founded for the purpose of encouraging the technology, chemistry and science of leather on a worldwide basis. It is therefore appropriate that we recognise the achievements of those of stature in our industry who have contributed significantly to our global understanding of the leather industry and its by-products. The IULTCS Merit Award is given biennially by the IULTCS Executive to an individual, whose past or current endeavours have had an extraordinary impact on our industry and provide an example for others to follow. Prof Jianzhong Ma fits this profile perfectly.

Prof Jianzhong Ma has published more than 240 academic articles on prestigious international peer-reviewed journals, such as Advanced Functional Materials, Angewandte Chemie International Edition, Green Chemistry, Carbohydrate Polymers, etc. Seven of them were selected by ESI high citation papers. More than 100 National Invention patents and 7 international invention patents have been authorized. He has published 9 books including 2 monographs, among which "Chemistry of Leather Finishing Materials" has been rated as one of the national top-quality courses. To formulate and revise 7 National and Industrial Standards. Currently, Prof. Jianzhong Ma's H-index (Reported by Web of Science) is 39 and total citation is more than 7056 times.

His extensive list of Practical Achievements is long and varied, with much of his time dedicated to the leather industry, helping to maintain sensible adjustments to testing methods as well as working on new technology for a better future for the leather industry worldwide. He is project leader of 973 pre-research Project of China, 863 Project of China, Key Project of the National Natural Science Foundation of China, General Project of the National Natural Science Foundation of China, National Key Research and Development Plan Project, and over 60 items of University-Enterprise Cooperation Research Projects.

Prof Jianzhong Ma has been actively involved with the development and industrialization of new leather tanning agents, retanning agents, finishing agents, fattening agents, and other chemicals, transferred to more than 40 enterprises at home and abroad.

Functional finishing agents such as cold resistant, hydrophobic and antifouling chemicals have been developed and put into practice. The achievement won the 2nd prize of national technological invention, as well as 2 types of 1st prize of provincial and ministerial technical invention.

He has presided over the national teaching team, national quality courses, national planning textbooks and national experimental teaching demonstration centre etc. He has cultivated more than 100 graduate students, including entrepreneurial talent of the national "Thousand Talents Plan", young top-notch scholar of the "Ten Thousand Talents Plan", and young scholar of Yangtze River Scholars. A large number of outstanding engineering talents have been delivered to the industry. He won the 2nd prize of national teaching achievement.

Stahl's innovations driven by sustainability

With the rise of both electric and self-driving, cars are becoming quieter and anti-squeak and rattle materials are becoming increasingly important. At the same time, improved anti-stain performance is required, because of the current trend for pale-colored car seats. Therefore, we have developed Stay Clean. This low-VOC coating technology protects pale-colored leather and vinyl surfaces against common stains, such as dye from jeans, spilled coffee and dirt. Our solution also makes surfaces low-squeak, which is a great asset as global research has shown that a squeaking car interior is one of the biggest annoyances among car owners. Another trend in car interior is the popularity of matt surfaces. Therefore, we have developed PolyMatte®. This non-squeaking solution provides a luxurious feel to the finished article in combination with flexibility and scratch and abrasion resistance. Our portfolio contains many products, varying from beamhouse products, tanning systems to finishes, duller concentrates, crosslinkers and thickeners to leveling agents, defoamers, colorants and hand modifiers. Our most sustainable option is Green PolyMatte®, which is based on rapeseed oil (20%) instead of crude oil-derived intermediates. If you would like to know what our Stahl solutions for automotive can do for your business, please visit **www.stahl.com** or contact us at: **alexander.campbell@us.stahl.com**.

If it can be imagined, it can be created

Stay Clean

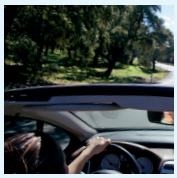

Low-VOC

PolyMatte®

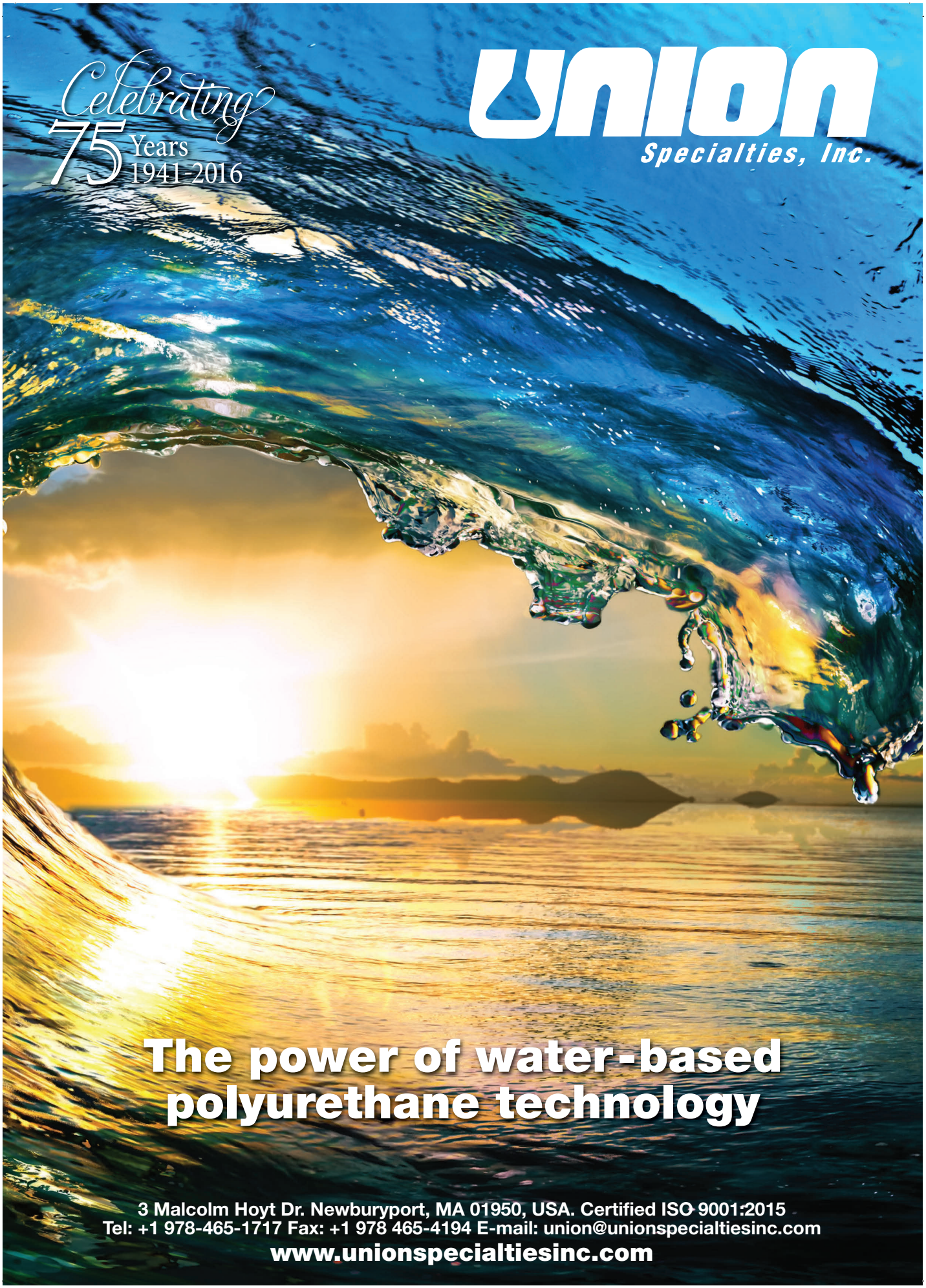
Celebrating
75 Years
1941-2016
UNION
Specialties, Inc.
The power of water-based polyurethane technology
3 Malcolm Hoyt Dr. Newburyport, MA 01950, USA. Certified ISO 9001:2015
Tel: +1 978-465-1717 Fax: +1 978 465-4194 E-mail: union@unionspecialtiesinc.com
www.unionspecialtiesinc.com

Lifelines

Min Gu is studying for her Master's degree at the College of Biomass Science and Engineering, Sichuan University, China.

Xiaoxia Zhang has a Master's degree and now she is studying as a doctor candidate at the College of Biomass Science and Engineering, Sichuan University, China.

Yuanzhi Zhang, see *JALCA* **115**, 279, 2020.

Songcheng Xu has a PhD at the College of Biomass Science and Engineering, Sichuan University, China.

Guoying Li, see *JALCA* **116**, 100, 2021.

S. Nithiyanantha Vasagam is working as a senior Principal Scientist at CSIR-Central Leather Research Institute (CSIR-CLRI) and has 22 years of experience in the field of Information Science & Technology. He received his Master of Computer Science from Madurai Kamaraj University, Madurai in the year 2000. His areas of interest include Image Processing, Artificial Neural Networks, Artificial Intelligence, Machine Learning.

M. Sornam is Professor in the Department of Computer Science, University of Madras. She received her MSc in Mathematics from the University of Madras in 1987, Master's Degree in Computer Applications from the University of Madras in 1991 and received her Ph.D in 2013 from University of Madras. She has published 112 papers in Indian and international journals, presented at national and international seminars, organized & participated in 56 workshops/seminars. Her area of specializations are Artificial Neural Networks, Artificial Intelligence, Machine Learning, Deep Learning and Image processing.

Pinar Caglayan graduated from Biology Department, Ataturk Faculty of Education, Marmara University. She received MSc, and PhD Degrees in Biology from Institute of Pure and Applied Sciences, Marmara University. She was an Erasmus student in Department of Microbiology and Parasitology, Faculty of Pharmacy, Sevilla University, Spain (2008-2009). Associated Professor Pınar Caglayan has been working at Division of Plant Diseases and Microbiology, Marmara University since 2011. Her research interests are moderately halophilic bacteria, extremely halophilic archaea, antimicrobial agents, hide microbiology, electric current applications on microorganisms.

Cigdem Kilicarislan Ozkan has been working in the Leather Engineering Department of Ege University since 2010. She completed her PhD in 2018. Her research activities and fields of interests are sustainable tanning materials, tannin extraction techniques, modification of biopolymers and leather technologies.

Letter to the Editor

Dear Editor,

I feel it necessary to register my disappointment in the paper: "Application of Acid Protease for Eco-friendly Pre-Treatment of Goat Skin to Improve Antimicrobial Finish using Herbal Natural Extracts".

The use of the term "Finish" in the leather industry implies a process following completion of tanning and retanning. It is therefore not clear whether the antimicrobial application was made on the pelt or on leather. One has to make the assumption that the application was on the untanned skin following enzyme treatment as there is reference to "alternative to conventional wet chemical treatment" and no documentation of tan or retan process. If so, then the need for antimicrobial processing following acid protease treatment is moot. There is no need for preservation treatment at this stage and immediate processing through tanning and retanning would in any case wash away most of the antimicrobials. Furthermore, the rationale for the research undertaken - "leather is highly prone to microbial proliferation and biodeterioration" - is simply false. Intact leather artifacts from centuries ago belie this statement. Hides, skins or pelts - yes; leather - no.

I also feel it necessary to speak specifically to the incorrect interpretation of the "zone of inhibition" technique for evaluating antimicrobial effects. "Growth" or "No Growth" must be evaluated on the leather. Zone of inhibition is correctly interpreted as the ability of an antimicrobial to diffuse into the Agar to exhibit effect and NOT for the protection of a sample against microbial attack. In fact, there should be less protection of the skin or leather as antimicrobial substance is lost to the matrix. The continued use of this technique in our industry to show efficacy of antimicrobials in protecting a substrate is simply wrong.

Sincerely,
Dr. Elton Hurlow
Past President ALCA / Past President IULTCS

INDEX TO ADVERTISERS

WARDROBE MALFUNCTION

LEATHER. IF WE DON'T USE IT, WE DO MORE THAN JUST LOSE IT.

From food to fashion, a burger and shake is just the start of the story of waste and recklessness. We live in a world where the cheap and easy option is to throw away the byproducts of our society. Instead we crop new land, drill or frack for short lived replacements. Isn't it time to shake things up, to think slow instead of fast. To think of our future and that of the planet?

300M HIDES COME FROM THE MEAT & DAIRY INDUSTRIES EVERY YEAR

60% IS USED FOR LEATHER. THE REST IS JUST TROWN AWAY

THAT IS **120M** 3M TONNES OF LANDFILL & 2.7M TONNES OF GREENHOUSE GASES. EVERY YEAR.

THE FASHION INDUSTRY PRODUCES

144 BILLION ITEMS OF CLOTHING EVERY YEAR

WE NEED 3.5M ACRES OF FOREST, JUST TO RE-CAPTURE THE CARBON CREATED BY THIS WASTE.

65% OF ALL OUR CLOTHES ARE PLASTIC, SOURCED THROUGH DRILLING & FRACKING

EACH HIDE COVERS **4 SQM**

WE WASTE NEARLY **480 MILLION SQM**

OF MATERIAL EACH YEAR, ENOUGH TO COVER

78,000 FOOTBALL PITCHES

OR TO PUT SHOES ON THE FEET OF

EVERY MAN, WOMAN & CHILD IN AFRICA

AND ONE LEATHER ITEM CAN LAST A LIFETIME

TO JOIN THE DISCUSSION FIND US AT: CHOOSEREALLEATHER.COM


www.CHEMTAN.com
Made with
WATERPROOF
TECHNOLOGY
CHEMTAN
Tel: (603) 772-3741 • Fax: (603) 772-0796 • www.CHEMTAN.com